iScience

CellPress
OPEN ACCESS

Article

Elements of the ERAD ubiquitin ligase Doa10 regulating sequential poly-ubiquitylation of its targets

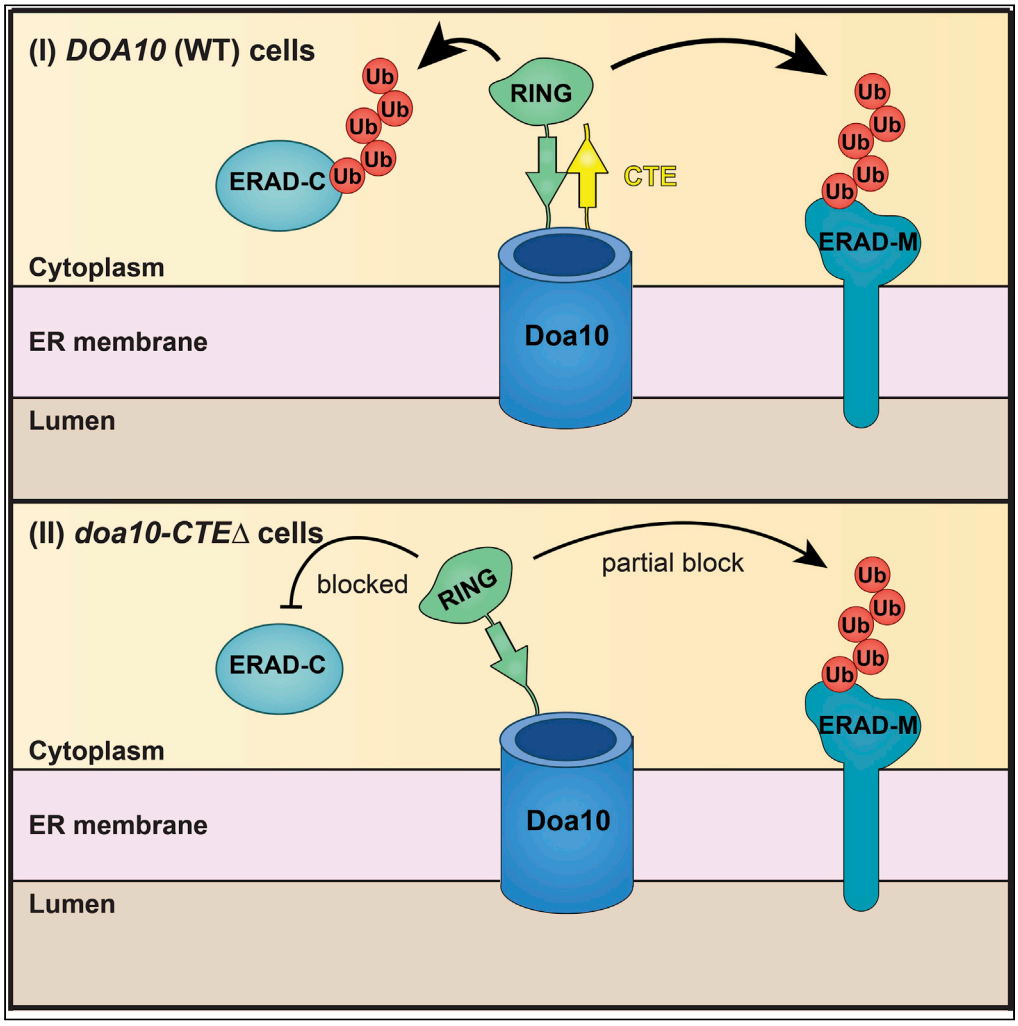

Adrian B. Mehrtash, Mark Hochstrasser

mark.hochstrasser@yale.edu

Highlights

The conserved Doa10 C-terminus promotes E3-mediated activity of Ubc6

The minimal E2-binding region of Doa10 includes TMs 1–9

The N- and C-terminus of Doa10 interact, likely forming an ERAD protein channel

Mehrtash & Hochstrasser, iScience *25*, 105351
November 18, 2022
https://doi.org/10.1016/j.isci.2022.105351

iScience

CellPress
OPEN ACCESS

Article

Elements of the ERAD ubiquitin ligase Doa10 regulating sequential poly-ubiquitylation of its targets

Adrian B. Mehrtash[1] and Mark Hochstrasser[1,2,3,*]

SUMMARY

In ER-associated degradation (ERAD), misfolded ER proteins are degraded by the proteasome after undergoing ubiquitylation. Yeast Doa10 (human MARCHF6/TEB4) is a membrane-embedded E3 ubiquitin ligase that functions with E2s Ubc6 and Ubc7. Ubc6 attaches a single ubiquitin to substrates, which is extended by Ubc7 to form a polyubiquitin chain. We show the conserved C-terminal element (CTE) of Doa10 promotes E3-mediated Ubc6 activity. Doa10 substrates undergoing an alternative ubiquitylation mechanism are still degraded in CTE-mutant cells. Structure prediction by AlphaFold2 suggests the CTE binds near the catalytic RING-CH domain, implying a direct role in substrate ubiquitylation, and we confirm this interaction using intragenic suppression. Truncation analysis defines a minimal E2-binding region of Doa10; structural predictions suggest that Doa10 forms a retrotranslocation channel and that E2s bind within the cofactor-binding region defined here. These results provide mechanistic insight into how Doa10, and potentially other ligases, interact with their cofactors and mediate ERAD.

INTRODUCTION

The endoplasmic reticulum (ER) is a continuous membrane system that includes the peripheral ER and nuclear envelope (NE). The ER is a major site for protein synthesis and maturation of membrane and secreted proteins in eukaryotes (Ghaemmaghami et al., 2003). Maintaining protein homeostasis at the ER is therefore crucial, and eukaryotes have developed multiple quality control mechanisms to prevent the accumulation of misfolded proteins in the ER (Babour et al., 2010; Braakman and Hebert, 2013; Ruggiano et al., 2014; Satpute-Krishnan et al., 2014; Szoradi et al., 2018; Wu et al., 2014). In ER-associated degradation (ERAD), proteins are ubiquitylated at the ER and subsequently degraded by the proteasome (Mehrtash and Hochstrasser, 2019). Membrane and soluble luminal proteins targeted by ERAD must undergo membrane extraction into the cytoplasm before or during proteasome-mediated degradation in a process called retrotranslocation (Mehrtash and Hochstrasser, 2019; Tsai et al., 2002).

The ERAD pathways selectively target misfolded proteins as well as regulatory proteins in response to different cellular stimuli. In the budding yeast *Saccharomyces cerevisiae*, three ER-resident ubiquitin ligase complexes are responsible for the majority of ERAD: the canonical Doa10 and Hrd1 complexes as well as the more recently characterized Asi complex, which is restricted to the inner nuclear membrane (INM) (Bordallo et al., 1998; Foresti et al., 2014; Hampton et al., 1996; Khmelinskii et al., 2014; Swanson et al., 2001). Collectively, these enzyme complexes target a diverse array of substrates. Doa10 mainly recognizes ERAD substrates with proteolytic targeting elements ("degrons") in the cytoplasm/nucleoplasm (ERAD-C) (Huyer et al., 2004; Metzger et al., 2008; Ravid et al., 2006) whereas Hrd1 recognizes ERAD substrates with degrons in the ER lumen (ERAD-L) or ER membrane (ERAD-M) (Carvalho et al., 2006; Gauss et al., 2006; Sato et al., 2009). Although Hrd1 is largely excluded from the INM, the Asi complex is capable of recognizing ERAD-M substrates in this cellular compartment (Deng and Hochstrasser, 2006; Natarajan et al., 2020; Ruggiano et al., 2014).

The primary component of the Doa10 complex is the E3 ubiquitin ligase Doa10, a large polypeptide that localizes throughout the ER/NE, including the INM, and contains 14 transmembrane helices (TMs) and an N-terminal RING-CH domain (Deng and Hochstrasser, 2006; Kreft et al., 2006). Doa10-mediated ubiquitylation almost always requires two different E2 ubiquitin-conjugating enzymes, Ubc6 and Ubc7 (Chen et al., 1993;

[1]Department of Molecular, Cellular, & Developmental Biology, Yale University, New Haven, 06520 CT, USA

[2]Department of Molecular Biophysics & Biochemistry, Yale University, New Haven, CT 06520, USA

[3]Lead contact

*Correspondence: mark.hochstrasser@yale.edu

https://doi.org/10.1016/j.isci.2022.105351

Swanson et al., 2001). These E2s use a sequential ubiquitylation mechanism where Ubc6 attaches an initial ubiquitin molecule to a substrate ("priming") that is subsequently elongated by Ubc7 to form a polyubiquitin chain (Weber et al., 2016). Following substrate ubiquitylation, soluble substrates of Doa10 are directly degraded by the proteasome; however, membrane-embedded substrates must initially undergo membrane extraction into the cytoplasm. This extraction step –known as retrotranslocation– requires the AAA+ ATPase Cdc48 and its associated factors Ufd1 and Npl4 (Mehrtash and Hochstrasser, 2019; Ravid et al., 2006). The ERAD E3 ligases and the Derlin rhomboid pseudoproteases have been proposed to participate directly in membrane extraction (Natarajan et al., 2020; Neal et al., 2018; Schmidt et al., 2020; Stein et al., 2014; Swanson et al., 2001), potentially by forming retrotranslocation channels (Rao et al., 2021; Wu et al., 2020).

The Doa10 pathway degrades proteins with diverse characteristics in multiple cellular compartments, including soluble proteins in the cytoplasm and nucleoplasm as well as membrane proteins throughout the ER/NE (Mehrtash and Hochstrasser, 2019). These include misfolded protein quality control substrates as well as regulatory proteins whose levels must be tightly regulated. For example, the Doa10 pathway promotes the degradation of Erg1, an essential enzyme in the sterol biosynthetic pathway, in response to high sterol levels (Foresti et al., 2013). The human ortholog of Doa10, MARCHF6/TEB4, similarly regulates the abundance of sterol biosynthetic enzymes in response to sterol levels, including the two rate-limiting enzymes squalene monooxygenase (the human ortholog of Erg1) and HMG-CoA reductase (Chua et al., 2017; Foresti et al., 2013; Zelcer et al., 2014). Doa10 also mediates the degradation of mislocalized proteins, such as those originally destined for the mitochondria or lipid droplets (Dederer et al., 2019; Matsumoto et al., 2019; Ruggiano et al., 2016; Shakya et al., 2021). Although certain characteristics of Doa10-dependent degrons have been defined (Chua et al., 2017; Furth et al., 2011; Johnson et al., 1998; Kats et al., 2018; Kim et al., 2013), the functional domains in Doa10 involved in substrate recognition remain completely unknown and no direct substrate interaction with Doa10 has been reported. Moreover, it is unclear why the Doa10 pathway requires two E2 enzymes and how these E2s operate within the same protein complex.

To identify regions within Doa10 responsible for particular functions, we first investigated the highly conserved 16-residue C-terminal element (CTE), an element required for the turnover of most substrates (Zattas et al., 2016). These analyses revealed that the CTE contributes to but is not essential for the turnover of the ERAD-M substrates Ubc6 and Sbh2, which exhibit only partial degradation defects in CTE mutant cells. We show the CTE is required specifically for Doa10-mediated activity of Ubc6. Unlike most Doa10 substrates, E3-mediated activity of Ubc6 is not needed for efficient ubiquitylation of Ubc6 and Sbh2, enabling their turnover in CTE mutant cells. Truncation analysis of Doa10 revealed the last four TMs (TMs 11–14) are not essential for ERAD-M turnover; by contrast, a mutant lacking the last five TMs of Doa10 (TMs 10–14), while still able to bind its cofactors (Ubc6, Cue1, and Ubc7), is degradation-deficient. The minimal uninterrupted cofactor-binding region of Doa10 was determined to include TMs 1–9. Structural predictions for Doa10 and its orthologs using AlphaFold2 revealed several interesting features, the most prominent being a large central channel formed from the 14 TMs of Doa10. Of interest, the conserved CTE is predicted to interact with the stem of the catalytic RING domain and TM1 of Doa10. We provide support for this interaction through mutagenesis and degradation analyses, including striking intragenic suppression involving two residues predicted to form a saltbridge. The CTE and RING-CH domain are predicted to form a linked structural motif that could provide insight into the unique catalytic properties of Doa10. Moreover, AlphaFold-Multimer predictions for Doa10 with Cue1, Ubc7, and Ubc6 suggest cofactor binding occurs outside of the central Doa10 channel and in the minimal cofactor-binding region defined here. Overall, this study defines critical functional regions within Doa10 and provides mechanistic insights into how a conserved ERAD complex facilitates E2-E3 interactions and mediates substrate ubiquitylation.

RESULTS

The CTE is required for normal turnover kinetics of Doa10 substrates

Mutation or deletion of the CTE (Figure 1A) blocks the turnover of most Doa10 substrates (Scheffer et al., 2019; Zattas et al., 2016). The CTE is highly conserved, and it is also required for the function of the human ortholog of Doa10, MARCHF6/TEB4 (Zattas et al., 2016), suggesting the CTE has a crucial and conserved function in the Doa10 pathway. We therefore performed a more detailed degradation analysis of the two substrates apparently unaffected in CTE mutant cells, Ste6* and Ubc6 (Zattas et al., 2016). Ste6 is a membrane protein that localizes to the cell surface and contains 12 TMs and two nucleotide-binding domains (NBDs) (Loayza et al., 1998). The truncation variant Ste6* contains a misfolded NBD2 that results in ER retention and degradation (Loayza et al., 1998). Because Ste6* turnover is regulated by at least three different ubiquitylation pathways

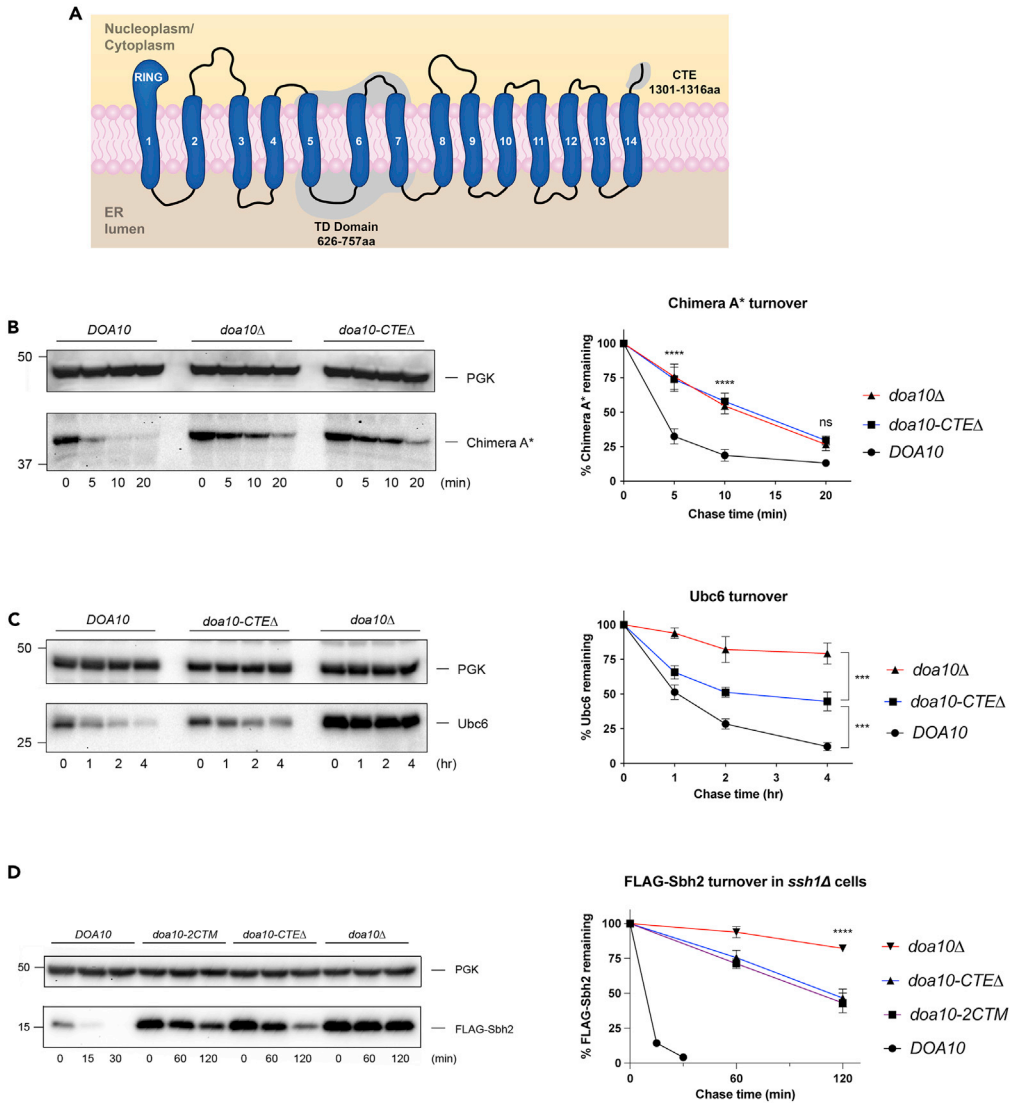

Figure 1. The CTE is required for normal turnover kinetics of Doa10 substrates

(A) Membrane topology of *S. cerevisiae* Doa10 highlighting three conserved regions important for Doa10 function. These include an N-terminal RING domain, the TEB4-Doa10 (TD) domain, and the C-terminal element (CTE).

(B) Cycloheximide chase analysis of Chimera A*. Following addition of cycloheximide (CHX), cells at the indicated time points were lysed and analyzed by anti-HA and anti-Pgk1 (PGK) immunoblotting. The graph (right panel) represents data as mean ± SEM from three experiments, ****$p < 0.0001$, two-way ANOVA with Tukey's post hoc analysis. Band intensities were normalized to the PGK loading control.

(C) Degradation of Ubc6 was analyzed as in panel B except CHX-chase analysis was performed on endogenous Ubc6, which was detected by anti-Ubc6 immunoblotting. The graph (right panel) represents data as mean ± SEM from three experiments, ***$p < 0.001$, two-way ANOVA with Tukey's post hoc analysis.

(D) Degradation of Sbh2 was analyzed as in panel B, except CHX-chase analysis was performed on ectopically expressed FLAG-Sbh2 in *ssh1Δ* cells. FLAG-Sbh2 was detected by anti-FLAG immunoblotting. The doa10-2CTM mutant contains two point mutations in the CTE (G1309L, N1314A). The graph (right panel) represents data as mean ± SEM from three experiments, ****$p < 0.0001$, two-way ANOVA with Tukey's post hoc analysis.

(Stolz et al., 2013), we performed cycloheximide (CHX)-chase analyses of Chimera A*, a simplified Doa10 substrate that contains 2 TMs and the misfolded NBD2 from Ste6* (Guerriero et al., 2017). Chimera A* was stabilized to the same extent in *doa10* mutant cells lacking either all of Doa10 or the CTE, *doa10Δ* or *doa10(1–1291)*, respectively (Figure 1B). Thus, like the other ERAD-C substrates tested previously, Doa10-mediated turnover of Chimera A* requires a functional CTE (Zattas et al., 2016).

Although Doa10 primarily targets ERAD-C substrates, a few ERAD-M substrates have been characterized. The TA protein Ubc6 is an unusual Doa10 substrate in that it functions both as an E2 enzyme in the Doa10 complex and contains an ERAD-M degron (Kreft and Hochstrasser, 2011; Swanson et al., 2001; Walter et al., 2001). Initial degradation analyses suggested that Ubc6 turnover did not require the Doa10 CTE; however, further examination of Ubc6 turnover through cycloheximide (CHX)-chase analyses revealed deletion of the CTE partially blocked Ubc6 degradation (Figures 1C and S1). Of the many Doa10 substrates analyzed in CTE mutant cells (Zattas et al., 2016), we had only observed partial stabilization for Ubc6; all other substrates were completely dependent on the CTE for their Doa10-dependent turnover.

We next asked whether other substrates, particularly those with features similar to Ubc6, require the CTE for their turnover. Sbh2 is a component of the non-essential Ssh1 translocon complex in *S. cerevisiae* and like Ubc6, a TA protein that contains an ERAD-M degron (Finke et al., 1996; Habeck et al., 2015). Sbh2 is rapidly degraded by the Doa10 complex in cells lacking one of its binding partners, Ssh1 (Habeck et al., 2015). We performed CHX-chase analyses of Sbh2 in *ssh1Δ* cells bearing several different *doa10* mutant alleles. Either missense mutations (*doa10-2CTM*) or deletion (*doa10-CTEΔ*; C-terminal residues 1292–1319 removed) of the CTE partially blocks the turnover of Sbh2 (Figure 1D). Thus, the CTE, while contributing, is not essential for degradation of the two known ERAD-M substrates targeted primarily by the Doa10 pathway. Our data suggest there could be a potential link between ERAD substrate classification (ERAD-C or ERAD-M) and degree of sensitivity to CTE mutation. A functional CTE is required for the ubiquitylation of *Deg1*-containing Doa10 substrates, suggesting it has a role during substrate recognition or ubiquitylation (Zattas et al., 2016). The data presented here indicate the CTE contributes to the turnover of all Doa10 substrates. However, unlike most substrates, Ubc6 and Sbh2 turnover persists in CTE mutant cells compared to a *doa10* null strain, suggesting these substrates are recognized or ubiquitylated through an additional, distinct mechanism.

Ubc6 auto-ubiquitylation enables its turnover in CTE mutant cells

To gain insight into the mechanistic contributions of the CTE, we further investigated the degradation of Ubc6, which exhibits partial degradation defects in CTE mutant cells (Figure 1C). Ubc6 is a unique substrate that functions as a Doa10 cofactor, and its E2 catalytic activity is required for its turnover (Swanson et al., 2001; Walter et al., 2001). Doa10 likely contains a distinct Ubc6-binding site that allows Ubc6 to bind Doa10 and ubiquitylate substrates at a separate substrate-binding site. The conserved TD domain (Figure 1A) may represent one of these interaction sites as mutational analyses have identified several TD mutants that lead to Ubc6-specific degradation changes (Kreft and Hochstrasser, 2011). One of these is a point mutation in TM5, *doa10-E633Q*, which leads to very rapid degradation of both epitope-tagged Ubc6 and endogenous Ubc6 (Figure S2), likely by enhancing its association with the substrate-binding site of Doa10 (Kreft and Hochstrasser, 2011). Of interest, catalytically inactive Ubc6-HA(C87A) is degraded in *doa10-E633Q* cells only when active Ubc6 is present *in trans*, but it is highly stable in wild-type *DOA10* cells. (Kreft and Hochstrasser, 2011). These results suggest that inactive Ubc6-HA(C87A) occupying the substrate-binding site in the mutant Doa10(E633Q) protein can be efficiently ubiquitylated by active Ubc6 at the Ubc6-binding site (Figure 2A). Thus, this E3 point mutant offers a useful tool for analyzing Ubc6 turnover at the substrate-binding site where Ubc6 auto-ubiquitylation is no longer required for its turnover.

The degradation of inactive Ubc6-HA(C87A) in *doa10-E633Q* cells requires Doa10 E3 ligase (RING) activity as well as Ubc7 and Ubc6 E2 activity *in trans* (Kreft and Hochstrasser, 2011). We sought to determine whether inactive Ubc6-HA(C87A) turnover in the *doa10-E633Q* strain also requires a functional CTE. For this we introduced a second mutation into the chromosomal *doa10-E633Q* allele to inactivate the CTE in these cells, generating the mutant *doa10-E633Q,CTEΔ*. Consistent with previous studies (Kreft and Hochstrasser, 2011), inactive Ubc6-HA(C87A) was rapidly degraded in *doa10-E633Q* cells. Strikingly, degradation of Ubc6-HA(C87A) in the *doa10-E633Q,CTEΔ* strain was nearly completely blocked (Figure 2B), suggesting its ubiquitylation at the substrate-binding site requires the CTE. By contrast, active Ubc6-HA turnover proceeded in the double mutant (Figure 2C). Both active and inactive forms of Ubc6 are presumably recognized by Doa10 in a similar manner. This implies that the CTE is not specifically required for substrate recognition. In contrast to active Ubc6, which can undergo auto-ubiquitylation, degradation of inactive Ubc6-HA(C87A) strictly requires Ubc6 activity *in trans* in *doa10-E633Q* cells, as noted above (Kreft and Hochstrasser, 2011). Therefore, these results suggest auto-ubiquitylation of wild-type Ubc6 enables its turnover in *doa10-CTEΔ* cells.

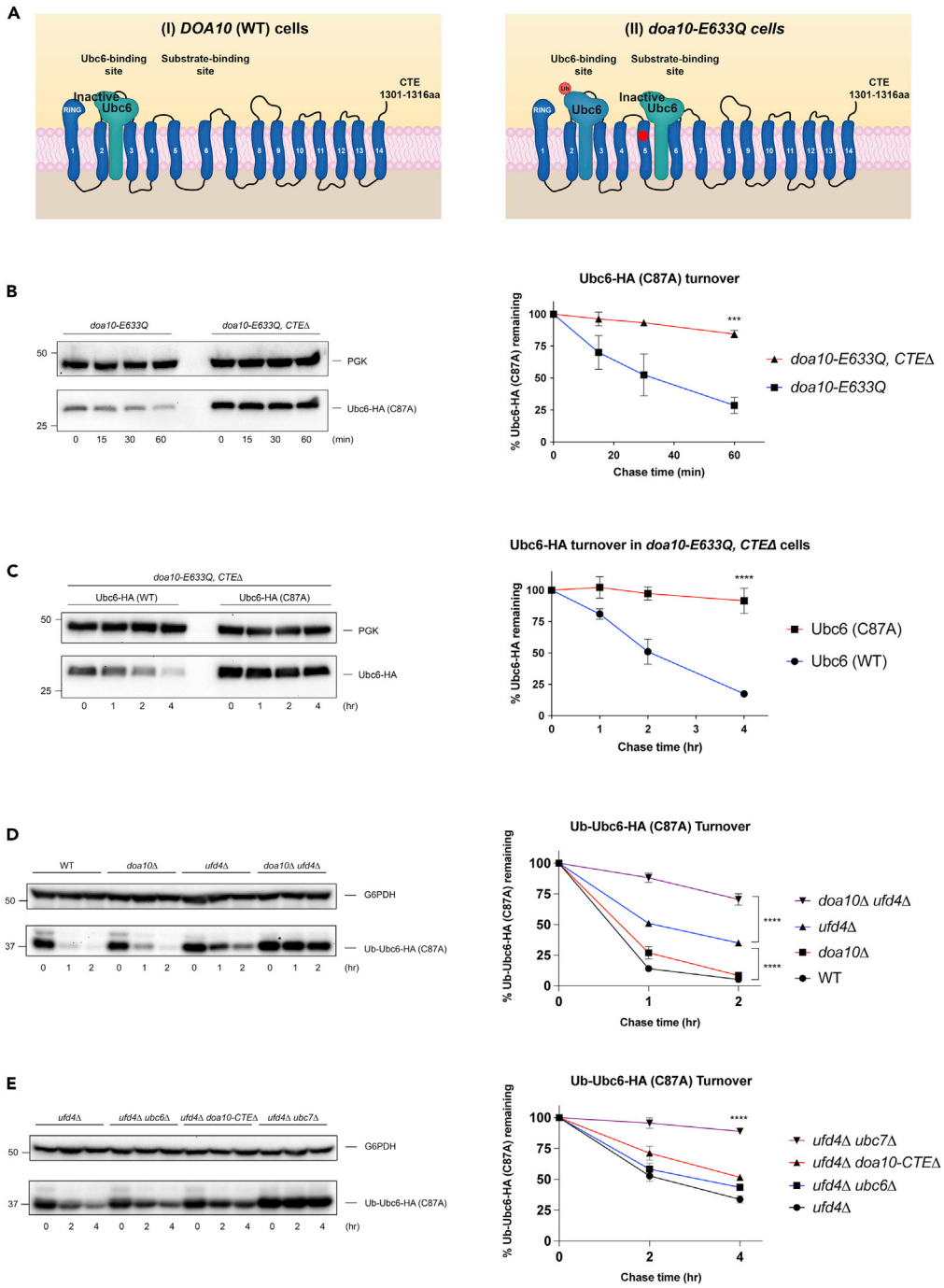

Figure 2. Ubc6 auto-ubiquitylation enables its turnover in CTE mutant cells

(A) Model for Ubc6 binding in wild-type (WT) and *doa10-E633Q* cells. (I) In WT cells, only a single Ubc6 molecule can interact with Doa10 at the "Ubc6-binding site." The Doa10 pathway does not degrade catalytically inactive (C87A) Ubc6 in this E3 context. We hypothesize that the *doa10-E633Q*mutation (II) allows redirection of Ubc6 from its normal Ubc6-binding site to the "substrate-binding site," where it can be efficiently ubiquitylated for degradation. As a result, expression together of active and inactive versions of Ubc6 in *doa10-E633Q* cells enables the ubiquitylation of inactive Ubc6 at the substrate-binding site. The locations of the Ubc6-and substrate-binding sites in this speculative model are hypothetical.

(B) Degradation of Ubc6-HA(C87A) was analyzed as in Figure 1B except CHX-chase analysis was performed on ectopically expressed Ubc6-HA(C87A) in the indicated yeast strains. Ubc6-HA(C87A) was detected by anti-HA immunoblotting. The graph (right panel) represents data as mean ± SEM from three experiments, ***p < 0.001, two-way ANOVA with Bonferroni's post hoc analysis.

Figure 2. *Continued*

(C) The degradation of Ubc6-HA and Ubc6-HA (C87A) was analyzed as in (B) except CHX-chase analysis was performed on ectopically expressed Ubc6-HA and Ubc6-HA(C87A) in *doa10-E633Q, ΔCTE* cells. The graph (right panel) represents data as mean ± SEM from four experiments, ****p < 0.0001, two-way ANOVA with Bonferroni's post hoc analysis.

(D) Degradation of Ub-Ubc6-HA(C87A) was analyzed as in Figure 1C except CHX-chase analysis was performed on ectopically expressed Ub-Ubc6-HA(C87A) in the indicated yeast strains. Ub-Ubc6-HA(C87A) and G6PDH were detected by anti-HA and anti-G6PDH immunoblotting, respectively. The graph (right panel) represents data as mean ± SEM from three experiments, ****p < 0.0001, two-way ANOVA with Tukey's post hoc analysis.

(E) Degradation of Ub-Ubc6-HA(C87A) was analyzed as in (D) in the indicated yeast strains.

To test this idea, we investigated whether bypassing the need for Ubc6 auto-ubiquitylation now allows inactive Ubc6(C87A) turnover in *doa10-CTEΔ* mutant cells. The attachment of a non-cleavable ubiquitin (Ub_{G76V}) to the N-terminus of inactive Ubc6, Ub_{G76V}-Ubc6(C87A), bypasses the need for Ubc6 activity and leads to efficient degradation initiated by Ubc7 alone (Weber et al., 2016). We speculated that N-terminal attachment of ubiquitin would also enable the turnover of inactive Ubc6-HA(C87A) in *doa10-CTEΔ* mutant cells. Notably, the turnover of Ub_{G76V}-Ubc6-HA(C87A) was only slightly stabilized in *doa10Δ* cells when evaluated using longer chase times than had been used previously (Figure 2D). Complete stabilization of Ub_{G76V}-Ubc6-HA(C87A) required combined deletion of *DOA10* and *UFD4*, an E3 ligase involved in the ubiquitin-fusion degradation (UFD) pathway (Johnson et al., 1995). To focus on Doa10-mediated degradation of Ub_{G76V}-Ubc6-HA(C87A), we performed additional CHX-chase analyses in cells lacking *UFD4* (Figure 2E). These experiments revealed that N-terminal attachment of ubiquitin to Ubc6-HA(C87A) was indeed able to overcome the degradation defect of the inactive E2 in *doa10-ΔCTE* cells.

Together, these data indicate the ability of Ubc6 to undergo auto-ubiquitylation enables its turnover when Doa10 lacks the CTE. Notably, while most substrates require Doa10 for Ubc6-mediated mono-ubiquitylation, Ubc6 can undergo mono-ubiquitylation independently of Doa10 (Schmidt et al., 2020; Weber et al., 2016). This distinct ubiquitylation mechanism enables Ubc6 degradation in CTE mutant cells.

E2 and CTE mutants differentially inhibit the turnover of a Doa10 ERAD-M substrate

The data presented to this point would imply that the Doa10 CTE is required for E3-mediated activity of Ubc6, the initial "priming" step during Doa10-mediated ubiquitylation. Unlike most substrates, Ubc6 and Sbh2 turnover might persist in CTE mutant cells because these substrates can be ubiquitylated through distinct mechanisms. Doa10 E3 activity is not required for auto-ubiquitylation of Ubc6, as just noted, and Sbh2 is efficiently ubiquitylated by Ubc7 alone, although *in vivo* Ubc6 is required for maximal degradation (Habeck et al., 2015; Weber et al., 2016). To investigate whether the CTE is required for Ubc6 function, we first compared the degradation kinetics of Sbh2 in *ssh1Δ* cells lacking either *UBC6* or the Doa10 CTE (Figure 3A). Although Sbh2 turnover is partially stabilized in either *ubc6Δ* or *doa10-CTEΔ* single mutants, the degree of Sbh2 stabilization is significantly greater in the CTE mutant, suggesting the CTE is not only required for Ubc6 function but could also contribute to another aspect of the Doa10 ERAD pathway.

We next tested whether the CTE is essential only for Doa10-mediated activity of Ubc6 toward Sbh2, as was shown for Ubc6. In fact, further stabilization of Sbh2 was observed in the *ubc6Δ doa10-CTEΔ* double mutant as compared to the *doa10-CTEΔ* single mutant (Figure 3B). Hence, Ubc6 also contributes to Sbh2 degradation in a way that is independent of the Doa10 CTE. Although Ubc6 primarily functions in the Doa10 ERAD pathway, Ubc6 can also function in the Hrd1 ERAD pathway (Lips et al., 2020). Because deletion of *HRD1* modestly stabilizes Sbh2 turnover (Habeck et al., 2015), we wondered whether additional stabilization of Sbh2 in the *ubc6Δ doa10-CTEΔ* double mutant is because of inhibition of Hrd1-mediated degradation of Sbh2 (as opposed to the Doa10 pathway). In support of this notion, we found that Sbh2 turnover was stabilized in the *hrd1Δ doa10-CTEΔ* double mutant (Figure 3C) to a degree similar to that in the *ubc6Δ doa10-CTEΔ* double mutant (Figure 3B). Moreover, deletion of *HRD1* in cells lacking *UBC6* had no impact on the turnover kinetics of Sbh2, suggesting Hrd1-mediated degradation of Sbh2 requires the E2 Ubc6. Together, these data indicate the CTE is indeed required for Doa10-mediated activity of Ubc6 toward Sbh2; however, greater stabilization of Sbh2 in the *doa10-CTEΔ* single mutant compared to the *ubc6Δ* single mutant suggests mutation of the CTE also impairs another aspect of Doa10 function.

The last 4 TMs of Doa10 are not essential for the turnover of its ERAD-M substrates

Besides the likely presence of a both general substrate-binding site and a Ubc6-binding site (Kreft and Hochstrasser, 2011), Doa10 likely has an additional binding site for the Ubc7 activator Cue1, which anchors

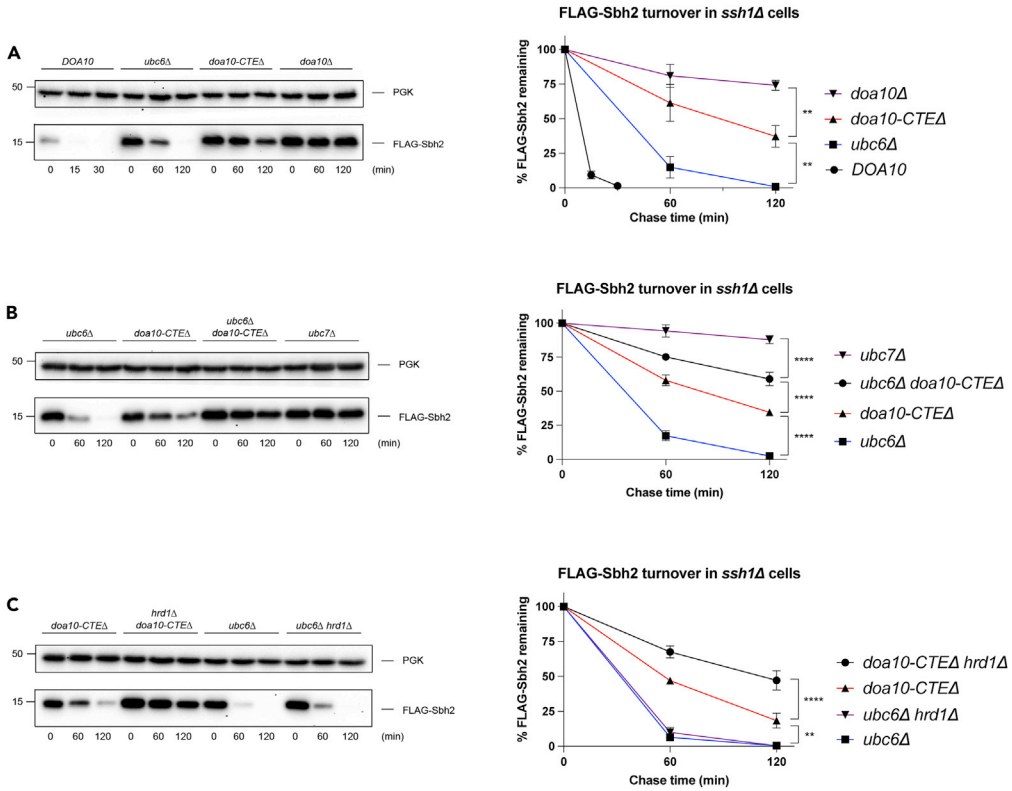

Figure 3. E2 and CTE mutants differentially inhibit turnover of a Doa10 ERAD-M substrate

(A) CHX-chase analysis of ectopically expressed FLAG-Sbh2 in *ssh1Δ* cells was done as in Figure 1D in the indicated yeast strains. The graph (right panel) represents data as mean ± SEM from three experiments, $^{**}p < 0.01$, two-way ANOVA with Tukey's post hoc analysis.

(B) The degradation of FLAG-Sbh2 was analyzed as in panel A in the indicated yeast strains. The graph (right panel) represents data as mean ± SEM from four experiments, $^{****}p < 0.0001$, two-way ANOVA with Tukey's post hoc analysis.

(C) The degradation of FLAG-Sbh2 was analyzed as in panel A in the indicated yeast strains. The graph (right panel) represents data as mean ± SEM from three experiments, $^{**}p < 0.01$, $^{****}p < 0.0001$, two-way ANOVA with Tukey's post hoc analysis.

Ubc7 to the ER membrane, stabilizes Ubc7 levels, and stimulates Ubc7 E2 activity (Bazirgan and Hampton, 2008; Biederer et al., 1997; Chen et al., 1993; Ravid and Hochstrasser, 2007; von Delbruck et al., 2016). The locations of these Doa10 binding sites have yet to be defined. To identify specific regions within Doa10 important for its function, we analyzed the turnover of Ubc6 in several chromosomally derived C-terminal truncation mutants of Doa10 (Figure 4A). Although all known Doa10 orthologs possess 12–16 TMs (Kreft et al., 2006), we found a Doa10 fragment, *doa10(1–1080)*, still capable of causing Ubc6 degradation despite only having TMs 1–10 (Figure 4B) (See Figure 5B for comparable expression of the truncation mutants). Ubc6 was partially stabilized in this truncation mutant, and further truncation that included Loop9-TM10, *doa10(1–1000)*, strongly stabilized Ubc6, indicating this region could have a central role in substrate turnover (Figure 4B). We also tested how these truncation mutants impact the turnover of another Doa10 ERAD-M substrate. Like the Ubc6 degradation results, turnover of Sbh2 was partially stabilized in the *doa10(1–1080)* mutant but fully stabilized in the *doa10(1–1000)* strain (Figure 4C). Therefore, truncation of Loop9-TM10 in Doa10 likely interferes with a crucial step in the Doa10 pathway, at least for ERAD-M substrates.

We speculated that disrupting Loop9-TM10 of Doa10 could either interfere with substrate binding or Doa10-mediated activity ("E3 stimulation") of its cognate E2 enzymes. To test whether C-terminal truncation through TM10 interferes with Doa10-mediated Ubc6 function, we analyzed the turnover of Ub_{G76V}-Ubc6-HA(C87A), a substrate that does not require Ubc6 function, in *ufd4Δ* cells. Ub_{G76V}-Ubc6-HA(C87A) was stabilized in *doa10(1–1000)* mutant cells, demonstrating that this mutant does not specifically interfere

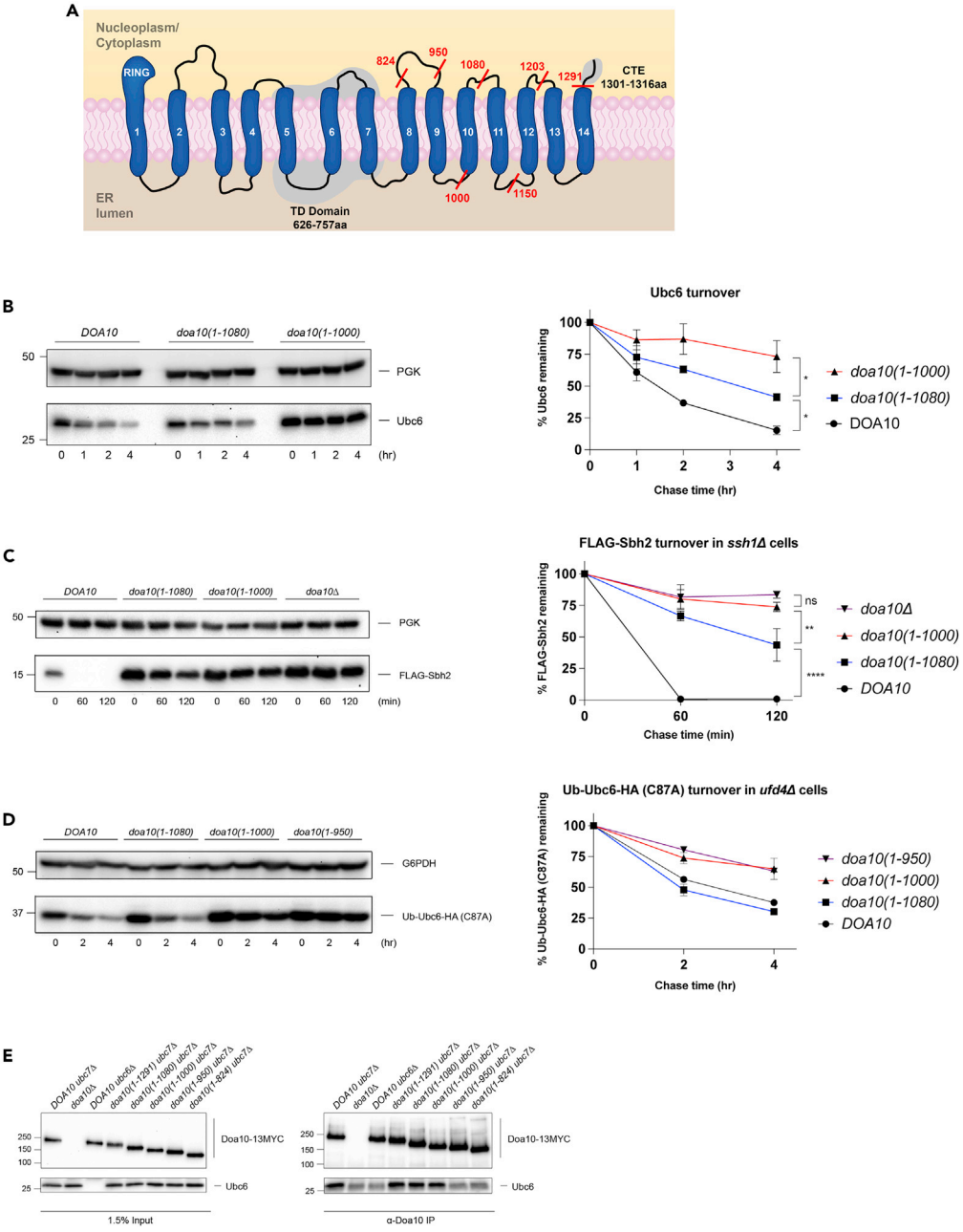

Figure 4. The last 4 TMs of Doa10 are not essential for turnover of its ERAD-M substrates

(A) Cartoon depicting the various C-terminal truncations of Doa10 used to analyze substrate turnover.

(B) CHX-chase analysis of endogenous Ubc6 was analyzed as in Figure 1C in the indicated yeast strains. The graph (right panel) represents data as mean ± SEM from three experiments, *p < 0.05, two-way ANOVA with Tukey's post hoc analysis.

(C) CHX-chase analysis of FLAG-Sbh2 was analyzed as in Figure 1D in the indicated yeast strains. The graph (right panel) represents data as mean ± SEM from three experiments, **p < 0.01, ****p < 0.0001, two-way ANOVA with Tukey's post hoc analysis.

(D) CHX-chase analysis of Ub-Ubc6-HA(C87A) was analyzed as in Figure 2D in the indicated yeast strains.The graph (right panel) represents data as mean ± SEM from four experiments.

(E) Co-immunoprecipitation (co-IP) analysis of Doa10 to investigate interactions between Doa10 and Ubc6. Microsomes were isolated from the indicated yeast strains and solubilized with digitonin. MYC-tagged Doa10 was immunoprecipitated with anti-Doa10 antibodies and the bound proteins were analyzed by anti-MYC and anti-Ubc6 immunoblotting. Note that there is a weak nonspecific band observed near Ubc6 in the anti-Doa10 IP (see lane 3).

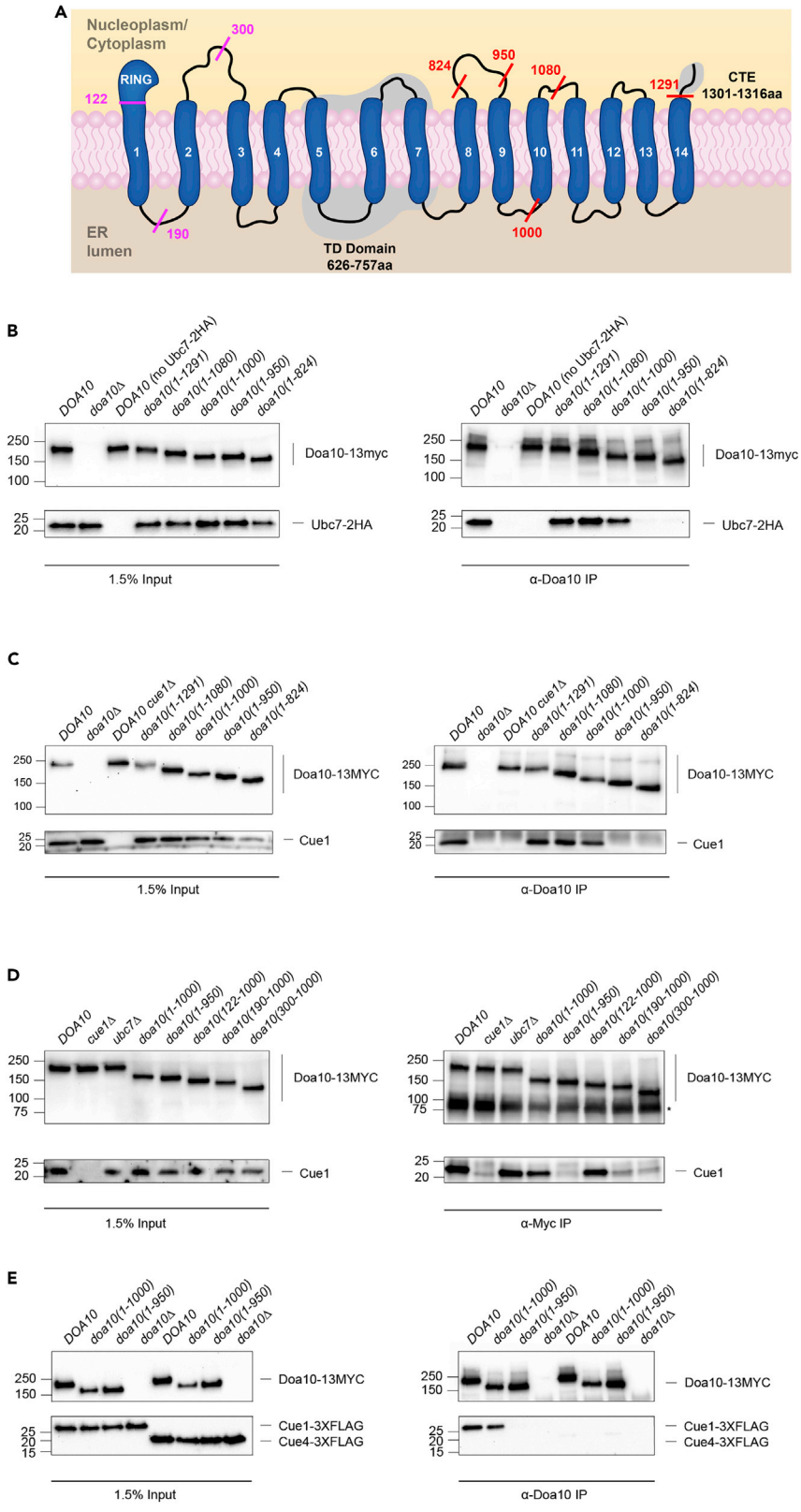
A
Nucleoplasm/
Cytoplasm
RING
122
300
824
950
1080
1291
CTE
1301-1316aa
1
2
3
4
5
6
7
8
9
10
11
12
13
14
ER
lumen
190
1000
TD Domain
626-757aa
B
DOA10
doa10Δ
DOA10 (no Ubc7-2HA)
doa10(1-1291)
doa10(1-1080)
doa10(1-1000)
doa10(1-950)
doa10(1-824)
250
150
100
Doa10-13myc
25
20
Ubc7-2HA
1.5% Input
α-Doa10 IP
C
DOA10
doa10Δ
DOA10 cue1Δ
doa10(1-1291)
doa10(1-1080)
doa10(1-1000)
doa10(1-950)
doa10(1-824)
250
150
100
Doa10-13MYC
25
20
Cue1
1.5% Input
α-Doa10 IP
D
DOA10
cue1Δ
ubc7Δ
doa10(1-1000)
doa10(1-950)
doa10(122-1000)
doa10(190-1000)
doa10(300-1000)
250
150
100
75
Doa10-13MYC
25
20
Cue1
1.5% Input
α-Myc IP
E
DOA10
doa10(1-1000)
doa10(1-950)
doa10Δ
250
150
Doa10-13MYC
25
20
15
Cue1-3XFLAG
Cue4-3XFLAG
1.5% Input
α-Doa10 IP

Figure 5. The minimal continuous cofactor binding region of Doa10 includes TMs 1–9

(A) Cartoon depicting the various C- and N-terminal truncations of Doa10 used to analyze Cue1 and/or Ubc7 binding.

(B) Co-IP analysis to investigate interactions between Doa10 and Ubc7 was performed as in Figure 4E except bound proteins were analyzed by anti-MYC and anti-HA immunoblotting. All strains in this panel except one (third lane) contain *pRH373-UBC7-2HA* integrated at the *TRP1* locus.

(C) Binding of Cue1 to Doa10 was analyzed as in panel B except bound proteins were analyzed by anti-MYC and anti-Cue1 immunoblotting.

(D) Binding of Cue1 to the indicated Doa10 mutants was analyzed as in panel C except MYC-tagged Doa10 was immunoprecipitated with anti-MYC antibodies.

(E) Binding of ectopically expressed Cue1-3XFLAG and Cue4-3XFLAG to Doa10 variants expressed from the endogenous locus was analyzed in the indicated yeast strains as in panel B except bound proteins were analyzed by anti-MYC and anti-FLAG immunoblotting.

with Ubc6 function (Figure 4D). Next, co-immunoprecipitation (co-IP) analysis was performed between endogenous Ubc6 and the truncation mutants to determine how these mutants impact Ubc6 binding. Binding was measured in strains lacking *UBC7* to prevent Ubc6 turnover and ensure Ubc6 levels are comparable in the different mutant strains. We found that the degradation-deficient *doa10(1–1000)* mutant, which lacks the CTE and TMs 11–14, was still capable of binding Ubc6 (Figure 4E); therefore, we speculated that disruption of this region interferes with some aspect of Ubc7 function, such as its ability to bind Doa10 or ubiquitylate substrates. Notably, truncation mutants lacking Doa10-TM9 [Doa10(1–950) and Doa10(1–824)] were incapable of interacting with Ubc6 (Figure 4E). We have not been able to detect binding between Doa10 and ERAD-C substrates, most likely because of the transient nature of these interactions; therefore, whether ERAD-C substrates are also capable of interacting with these truncation mutants is unclear and will likely require crosslinking experiments, such as those previously performed (Nakatsukasa et al., 2008).

The minimal continuous cofactor-binding region of Doa10 includes TMs 1–9

Our analyses of C-terminal truncation mutants of Doa10 suggested the region surrounding TM10 is crucial for Doa10 function. A loss of binding between Ubc7 and Doa10 was previously reported in the *doa10(1–950)* truncation mutant, which lacks TMs 9–14 (Kreft and Hochstrasser, 2011). Therefore, the degradation defects observed in *doa10(1–1000)* mutant cells, which lack TM10 and regions further C-terminal to it (Figure 5A), could also be related to impaired binding between Ubc7 and Doa10. To test this, we performed co-IP analyses between Doa10 and Ubc7 in the C-terminal truncation mutants of Doa10 (Figure 5B). While the truncation mutants lacking TM9 were indeed deficient in Ubc7-binding, continued binding of Ubc7 was seen for the less extensive truncation mutants, including the degradation-deficient *doa10(1–1000)* mutant. Therefore, removal of the region downstream of TM9 interferes with Ubc7 activity, but not binding between Ubc7 and Doa10. Given Ubc7 is recruited to the Doa10 complex by the cofactor Cue1 (Bagola et al., 2013), we also performed a similar binding analysis between Cue1 and Doa10. As seen for Ubc7, only the mutants lacking TM9 were deficient in Cue1-binding (Figure 5C). Because Cue1 recruits Ubc7 to the ER membrane, where it functions with Doa10, these results indicate their binding does not require TMs 10–14 of Doa10.

Notably, all three ERAD E3 ligase complexes in yeast require Cue1 and Ubc7 for substrate ubiquitylation (Biederer et al., 1997; Khmelinskii et al., 2014; Swanson et al., 2001); however, the location of their binding sites within the ERAD E3s is unknown. To identify the N-terminal end of the minimal cofactor-binding region of Doa10, we started with the *doa10(1–1000)* chromosomal mutant, whose product still can bind Cue1-Ubc7, and removed segments encoding N-terminal Doa10 sequences from the endogenous locus. We then performed co-IP experiments. The minimal truncation variant capable of binding Cue1 was *doa10(122–1000)*, a mutant lacking the catalytic RING-CH domain (Figure 5D). Further truncation of Doa10 from its N-terminus, such as deletion of TM1 (*doa10(190–1000)*), completely disrupted Cue1 binding. Therefore, the minimal Cue1-binding region of Doa10 encompasses TMs 1–9 and surprisingly, does not require the RING-CH domain, which is expected to activate E2∼ubiquitin transfer to substrate. Attempts to measure Ubc6 binding with the N-terminal truncation mutants of Doa10 were unsuccessful because of high background associated with the Doa10-Myc IP. Nevertheless, we have narrowed the location of the Ubc6-binding region to within the first 1000 residues of Doa10, which include TMs 1–9 (Figure 4E). Although it is uncertain if Ubc6 can interact with Doa10 truncations lacking N-terminal segments, we define the minimal cofactor-binding region of Doa10 capable of binding Cue1 (and by implication, Ubc7) as the segment bracketing TMs 1–9.

To verify the specificity of these co-IP interactions, we compared Doa10 binding by Cue1 and its paralog Cue4. Cue4 was chosen as a negative control because it is an ER membrane protein that has not previously been linked to ERAD, but it shares a high degree of sequence similarity with the Doa10-interacting region of Cue1 (residues 1–64) defined here, which includes its single transmembrane domain (Figure S3). Epitope-tagged versions of Cue1 and Cue4 were both stably expressed in yeast at similar levels, yet only Cue1 interacted with Doa10 (Figure 5E). Therefore, co-IP interactions under the conditions used are highly specific to proteins within the Doa10 complex.

The CTE and RING-CH domain of Doa10 are predicted to interact

To gain insight into the role of the functionally important regions analyzed in this study, we examined the predicted structure of Doa10 by AlphaFold2 (Figure 6A) (Jumper et al., 2021). This structural prediction revealed several interesting features, including a large apparent channel formed by the TMs of Doa10 (Figure 6B). The potential protein channel, which is partially lined by the conserved TD domain, could represent an ERAD channel that aids in substrate recognition and retrotranslocation. Moreover, the first (TM1) and last (TM14) TMs of Doa10 are juxtaposed, and the RING-CH domain and CTE are predicted to interact; an anti-parallel beta-sheet is formed by strands from the CTE and the stem just below the zinc-coordinating RING-CH domain, and several electrostatic interactions are predicted between these elements (Figure 6C). These terminal interactions enable the TMs to form a large transmembrane ring. Very similar interactions are predicted for the human and *Schizosaccharomyces pombe* orthologs of Doa10 (not shown). Given that the CTE is required for Doa10-mediated activity of Ubc6, the predicted interaction between the CTE and the catalytic RING-CH domain suggests the CTE has a direct role in E2 activation and substrate ubiquitylation.

To determine whether the location of the CTE is crucial for its function, we appended the CTE to the end of the *doa10(1–1080)* mutant, which is otherwise functionally similar to the *doa10-CTEΔ* mutant in that it also retains partial activity against ERAD-M substrates of Doa10 (Figure 4). We monitored ERAD-C turnover, which is fully dependent on the CTE, using a degradation-sensitive growth assay. Because the membrane substrate *Deg1*-Vma12-Ura3 is the only source of Ura3 in these cells, yeast grow poorly on media lacking uracil when it is rapidly degraded via the Doa10 pathway, but strong growth is seen when Doa10 is eliminated (Kreft and Hochstrasser, 2011). We found that the *doa10(1-1080-CTE)* mutant was unable to rescue ERAD-C turnover (Figure 6D). Moreover, attachment of the wild-type CTE to the C-terminus of the *doa10-2CTM* mutant protein also failed to rescue ERAD-C turnover, indicating the CTE must be precisely located within the Doa10 protein to perform its function (Figure 6D).

We next tested whether potential RING-CH-binding residues are important for CTE function. To this end, we focused on mutating charged or polar residues of the CTE that are predicted to interact with the RING-CH domain (K1308, E1313, N1314, E1318). The only point mutant that strongly stabilized *Deg1*-Vma12-Ura3 turnover was the *doa10-N1314A mutant* (Figures S4 and S5) (Zattas et al., 2016), which is expected to disrupt the predicted hydrogen bond between N1314 and H54. Of interest, among the polar or charged CTE residues predicted to interact with the RING domain, N1314 is the most conserved and the Asn-His interaction is also predicted by AlphaFold2 to occur in the human ortholog of Doa10, MARCHF6.

Because the *Deg1*-Vma12-Ura3 spot assay only detects mutants that strongly impair Doa10 function, we also performed spot assays with the soluble *Deg1*-Ura3 reporter, which can identify mutants that produce very modest degradation defects (Figures 6E and S6). We found the more conservative N1314D mutation also impairs substrate turnover, thereby highlighting the importance of this conserved residue. Of interest, AlphaFold2 prediction of the Doa10-N1314A mutant protein suggested this mutation leads to local structural rearrangements while still maintaining the overall CTE-RING interaction (Figure S7). We were unable to validate the predicted CTE-RING interaction through *in vitro* binding experiments using soluble versions of the CTE and RING-CH (not shown). We anticipate that the proximal location of these elements within endogenous Doa10 helps to facilitate this interaction. In particular, TM1 and TM14 are predicted to interact through hydrophobic and hydrophilic interactions near the cytosolic/ER membrane boundary, which includes an ionic interaction between E1304 and K119 (Figure 6F).

To test whether the predicted interaction between the regions near TM1 and TM14 is important for Doa10 function, we analyzed point mutations at E1304 of the CTE. Notably, a negatively charged residue (D/E) is absolutely conserved at this position among evolutionarily distant species (Zattas et al., 2016). Based on growth assays, the opposite charge E1304R mutation produced the strongest defect on *Deg1*-mediated

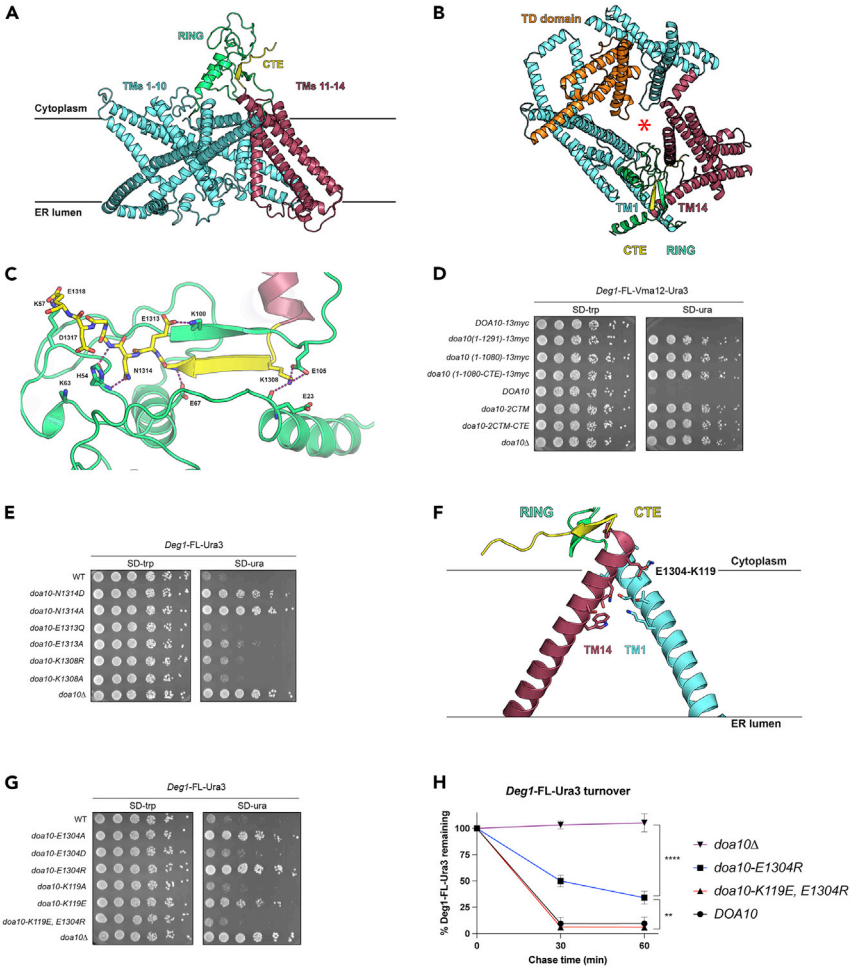

Figure 6. The CTE and RING-CH domain of Doa10 are predicted to interact

(A) Side view of the AlphaFold2 model for Doa10 displaying the RING domain (residues 6–112) in green, TMs 1–10 (residues shown are 113–225, 463–825, 961–1052) in cyan, TMs 11–14 (residues 1095–1306) in maroon, and the cytoplasmic portion of the CTE (residues 1307–1318) in yellow. Boundaries of the membrane bilayer are approximate. Residues not noted here are hidden for image clarity.

(B) AlphaFold2 model for Doa10 viewed from the cytoplasmic side of the ER membrane. Regions are displayed as in (A) except the conserved TD domain (608–761) is orange. A red *asterisk* highlights the location of the predicted Doa10 channel.

(C) Detailed cartoon representation of the RING-CTE motif as predicted by AlphaFold2. Electrostatic interactions between the RING finger and CTE are highlighted with dashed lines.

(D) Degradation-dependent yeast growth assay using the membrane substrate *Deg1*-Vma12-Ura3 expressed from the *MET25* promoter. Serial dilutions of the indicated strains transformed with the *TRP1*-marked *Deg1*-Vma12-Ura3 expression plasmid were spotted on the indicated media. The *doa10-2CTM* mutants contain two CTE mutations (G1309L, N1314A).

(E) Degradation-dependent growth assay as in (D) except the indicated yeast strains were transformed with the soluble substrate Deg1-FLAG-Ura3.

(F) AlphaFold2 model showing TM1 and TM14 of Doa10 viewed from inside the Doa10 channel. The dashed lines highlight the ionic interaction predicted between E1304 and K119. Other residues depicted include W1293, T1297, N1300 (TM14) and K127, T123, S120 (TM1).

(G) Degradation-dependent growth assay as in (E) using the indicated strains.

(H) CHX-chase analysis of Deg1-FL-Ura3. The graph represents data as mean ± SEM from three experiments, $^{**}p < 0.01$, $^{****}p < 0.0001$, two-way ANOVA with Tukey's post hoc analysis. Band intensities were normalized to the G6PDH loading control. See Figure S9 for a representative western blot of this data.

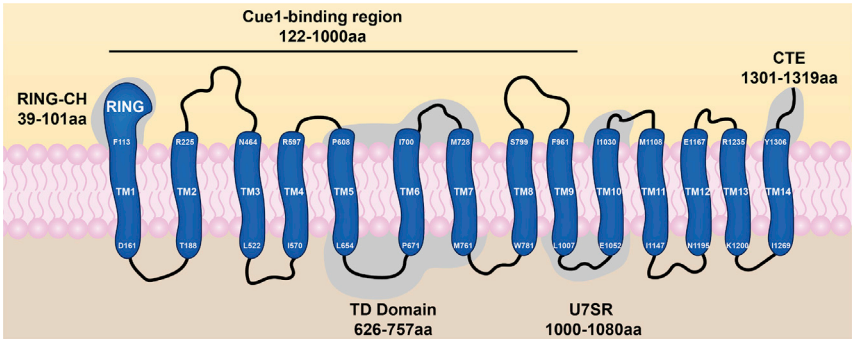

Figure 7. Topology model for *S. cerevisiae* Doa10 based on the AlphaFold2 prediction model

Doa10 contains 14 transmembrane helices (TMs) and both termini face the cytoplasmic side of the ER membrane. The catalytic RING-CH domain is located at the N-terminus whereas the C-terminal element (CTE) is at the C-terminus. The conserved TEB4-Doa10 (TD) domain contains TMs 5–7 as well as the loop regions between. Here, we also define a potential Ubc7-sensitive region (U7SR), which we predict is required for Doa10-mediated activity of Ubc7, and the Cue1-binding region encompassing TMs 1–9 of Doa10. Notably, because the AlphaFold2 structure lacks lipid molecules, the TM boundaries shown here are not definitive. A number of the predicted helices are remarkably long, most notably TM1 and TM5.

turnover, the E1304A mutation had an intermediate effect, and the E1304D mutation had no impact on either *Deg1*-Vma12-Ura3 or *Deg1*-Ura3 turnover (Figures 6G and S8). When the K119 residue in the N-terminal domain that is predicted to form a saltbridge with E1304 was mutated to an oppositely charged Glu residue, *Deg1*-Ura3 was also stabilized. Remarkably, introducing the K119E mutation into the *doa10-E1304R* allele completely restored Doa10 function based on growth assays and CHX-chase analysis (Figures 6G, 6H, S8, and S9). These results provide strong *in vivo* evidence supporting the AlphaFold2 structure prediction and suggest the interaction between the terminal domains of Doa10 is important for E3 function. We propose that the cytoplasmic ends of the terminal Doa10 transmembrane helices, TM1 and TM14, facilitate both formation of an exit channel –and are potentially part of a lateral gate– and interaction between the CTE and RING-CH domain. Overall, our genetic and biochemical analyses support key aspects of the AlphaFold2 structural prediction for Doa10, such as the formation of a long-range interaction between the CTE and RING-CH domain, that is crucial for E3-mediated ubiquitylation.

DISCUSSION

Since the initial discovery of Doa10 over twenty years ago, identification of regions within the E3 responsible for particular functions or protein interactions has been limited, with the major exception being the RING-CH domain (Swanson et al., 2001). RING fingers contain conserved cysteine and histidine residues that coordinate Zn^{2+} and mediate E2 binding (Metzger et al., 2014). They also contain a conserved "linchpin residue" that engages both ubiquitin and E2 through hydrogen bonding (Pruneda et al., 2012). The Doa10 RING domain contains a cysteine and histidine at coordinating positions four and five (RING-CH), respectively, and is therefore distinct from the classical RING-HC domain (Swanson et al., 2001). Moreover, the Doa10 RING-CH finger contains a suboptimal histidine residue as its linchpin, which appears to be inefficient at ubiquitin priming (Lips et al., 2020). On the other hand, the basal activity of Ubc6 is unusually high, and its enzymatic activity is minimally stimulated by the Doa10 RING *in vitro* (Lips et al., 2020). This could in part explain how Doa10 and Ubc6 mediate ubiquitin priming with a suboptimal RING linchpin residue. However, because full-length Doa10 significantly enhances Ubc6 activity (Schmidt et al., 2020), it is likely that additional regions contribute to proper E2/E3 pairing and Doa10-mediated stimulation of Ubc6.

In this study, we have characterized Doa10 elements involved in different aspects of sequential protein polyubiquitylation: ubiquitin priming as well as E2 and Cue1 cofactor binding (Figure 7). One focus of our analysis was the conserved CTE, an element we show is required for Doa10-mediated mono-ubiquitylation (ubiquitin priming). Thus, the CTE is essential for the degradation of most Doa10 substrates, i.e., those targeted for degradation through a sequential E2 mechanism involving Ubc6 and Ubc7 (Weber et al., 2016). Although Ubc6 and the CTE are absolutely required for Doa10-mediated ubiquitin priming, the CTE also likely contributes to Ubc7-mediated ubiquitin chain elongation. This was inferred from degradation analyses of the ERAD-M substrate Sbh2, which revealed that single mutants in either Ubc6 or the CTE differentially inhibit Sbh2 turnover (Figure 3). If the CTE were solely required for Doa10-mediated mono-ubiquitylation by Ubc6,

deletion of *UBC6* would be expected to produce a similar degradation defect to the CTE single mutant rather than the observed weaker effect. Although we provide strong genetic evidence that links the Doa10 CTE function to ubiquitin priming, it was still unclear if the CTE was involved directly in this process.

To gain insight into the underlying mechanism of the CTE in ubiquitin priming, we analyzed the predicted structure of Doa10 and its orthologs by AlphaFold2. There are several interesting features revealed from these structures. These include the relative location of the catalytic RING-CH domain and the CTE. Although these elements are encoded at the extreme N- and C-terminus of the protein, respectively, AlphaFold2 predicted a closely intertwined association between the two. The mutagenesis analyses performed here support the predicted CTE-RING-CH interactions. We also show the precise location of the CTE is crucial for its function (and presumably for binding to the RING-CH domain). Most importantly, intragenic suppression by complementary mutations of residues K119 and E1304 near the two ends of Doa10 yielded results consistent with their forming a functionally critical saltbridge. Doa10-K119 is not broadly conserved, but a similarly positioned saltbridge between human MARCHF6 residues D77 and K881 in the CTE is predicted by AlphaFold2. Thus, residues bringing together the N- and C-terminal domains of Doa10 might be co-evolving.

We predict interactions between the terminal TM1 and TM14 helices and their respective cytoplasmic tails facilitate specific binding between the CTE and RING-CH domain as well as Doa10 channel formation. The central channel predicted for Doa10 and its orthologs could potentially serve as a conduit for extracting transmembrane substrates of Doa10 from the ER. This function implies the presence of a lateral gate to allow membrane substrate entry into the channel. TM1 and TM14 might contribute to this gate, with the CTE-RING-CH domain association potentially acting as a dynamic clasp.

The exact function of the predicted CTE-RING-CH interaction is not certain; however, the presence of the CTE at the enzyme active site of Doa10 implies a direct role in substrate ubiquitylation. The CTE-RING binding motif appears to be conserved in Doa10 orthologs based on sequence conservation and structural predictions by AlphaFold2 (Jumper et al., 2021; Zattas et al., 2016). This was supported by a previous study that found mutation of a conserved asparagine in the CTE of human MARCHF6 (equivalent to yeast N1314) impaired E3 function (Zattas et al., 2016). Consistent with our findings here, a very recent paper reported biochemical evidence for direct CTE-RING binding in MARCHF6 (Nguyen et al., 2022). There are likely some differences in how the Doa10 and MARCHF6 CTEs function. For example, Nguyen et al. found that the MARCHF6 C-terminal domain (residues 870–910) was necessary and sufficient for binding to the human Ubc6 and Ubc7 E2 orthologs, whereas the equivalent Doa10 domain is not necessary for E2 binding (Figures 4 and 5). Further work is needed to determine whether the CTE in MARCHF6 is similarly required for E3-mediated mono-ubiquitylation. The CTE appears to be a motif exclusive to Doa10 orthologs based on sequence comparisons (Zattas et al., 2016). It is possible that it has evolved to couple the dynamics of the Doa10 protein exit channel with potentiation of RING-CH ubiquitylation activity.

In this study, we also sought to identify the regions within Doa10 responsible for either E2 or substrate binding. The locations of these Doa10 binding sites had been unknown, although the conserved TD domain was predicted to represent either an E2 or substrate-binding site (Kreft and Hochstrasser, 2011; Swanson et al., 2001). As Doa10 ERAD-M substrates are still degraded to some degree in cells lacking a functional CTE, we generated several C-terminal truncation mutants to identify other regions needed for substrate turnover. We found a mutant with only TMs 1–10 (TM11-14Δ) is functionally similar to a CTE mutant retaining all 14 TMs. It appears that the last four TMs are dispensable (at least for the tested substrates) except for the proper positioning of the CTE. This was an unexpected result given that all known Doa10 orthologs contain 12–16 predicted TMs (Kreft et al., 2006). Additional deletion of Loop9-TM10 in *doa10(1–1000)* produced a degradation defect similar to that in cells completely lacking *DOA10* (Figure 4). This degradation-deficient mutant is still capable of binding Ubc6, Cue1, and Ubc7 but lacks the ability to target ERAD-M substrates (even when "primed"). We predict the deletion of this region produces a specific defect in Ubc7 activity.

Moreover, we define the minimal cofactor-binding region of Doa10, namely the region capable of binding Ubc6, Ubc7, and Cue1, as the segment including TMs 1–9. The Doa10 RING domain was previously shown to interact weakly with Ubc6 and Ubc7 *in vitro* (Lips et al., 2020), yet we found it is not required for stable interactions between Doa10 and Cue1, the cofactor that recruits Ubc7 to the ER membrane and the Doa10 complex (Bagola et al., 2013; Biederer et al., 1997). We were unable to narrow the minimal continuous cofactor-binding region any further, as N-terminal truncation mutants lacking TM1 were incapable of

binding Cue1. We do not anticipate that this entire minimal binding region, which consists of residues 122–1000 and includes nine TMs, participates directly in protein-protein interactions. Instead, we imagine that cofactor binding is abrogated in the more extensive N-terminal truncations because of improper folding of subsequent domains or to the possibility that the critical binding elements happen to be near the ends of the linear polypeptide sequence.

We employed AlphaFold-Multimer (Evans et al., 2021) to predict the full structure of the Doa10 ligase complex and gain additional insight into cofactor binding. These predictions suggest cofactor binding occurs within the binding region we have defined experimentally. In particular, the TM segments of Cue1 and Ubc6 are located outside of the Doa10 channel near TM7, TM9, and Loop 8 (Figures S14 and S15). Of interest, Loop 8 is predicted to form an unusual globular domain near the cytosolic/ER membrane interface (Figure S16), where it interacts with both Cue1 and Ubc6 (Figure S15). These structures provide insight into how the *doa10(1–950)* truncation mutant, which lacks TM9 and part of Loop 8, disrupts cofactor binding. The first several N-terminal TM segments, which are required for cofactor association (Figures 4E and 5B), do not appear to participate directly in their binding, consistent with the assumption these TMs are needed for proper downstream TM insertion and folding. Notably, the cofactor-binding region defined here is the first known E2-binding site for an ERAD E3 in yeast. In mammalians cells, the ERAD E3 gp78 contains a UBE2G2 Binding Region (G2BR) (Das et al., 2009); however, the G2BR is a soluble domain and relatively small compared to the cofactor-binding region of Doa10. Although Ubc7 contains a mammalian ortholog that functions in ERAD, there is no apparent mammalian ortholog for the cofactor Cue1. Despite this, the ERAD accessory protein AUP1 appears to perform an analogous function (Smith et al., 2021). More work is needed to further understand E2-E3 pairing in mammalian orthologs of Doa10 and the other ERAD E3s.

In summary, we have provided mechanistic insights into how Doa10 and its E2 enzymes assemble into a functional membrane ubiquitin-ligase complex. Future experiments are needed to determine the exact mechanistic contributions of the RING-CTE motif and its function in other Doa10 orthologs. Moreover, structural studies are needed to validate the AlphaFold2 predictions. In these predicted structures, the TMs of Doa10 appear to form an ERAD protein channel, which likely contributes to substrate recognition and retrotranslocation. This channel is distinct from other recently proposed ERAD channels, which are formed from multiple proteins or polypeptide subunits (Rao et al., 2021; Wu et al., 2020). We predict substrate recognition occurs within the conserved TD domain (Kreft et al., 2006), which partially lines the putative Doa10 channel but also protrudes into the cytoplasm/nucleoplasm. Although Doa10 mediates Ubc6 retrotranslocation *in vitro* (Schmidt et al., 2020), primed versions of Ubc6 that are targeted by Ufd4 can be degraded (and presumably retrotranslocated) independently of Doa10 (Figure 2D). We anticipate it will be difficult to demonstrate retrotranslocase activity of Doa10 *in vivo* because there are several expected avenues for retrotranslocation (reviewed in (Mehrtash and Hochstrasser, 2019)). Alternative use of distinct protein retrotranslocation channels in different cellular compartments has also been reported (Flagg et al., 2021). It will be interesting to determine the retrotranslocation pathways involved in the degradation of different Doa10 substrates, particularly those that localize to the INM.

Limitations of the study

We determined that two Doa10 ERAD-M substrates exhibit partial degradation defects in CTE mutant cells, whereas ERAD-C substrate turnover is completely blocked. These results are likely because of differences in ubiquitylation mechanism as opposed to ERAD substrate class per se. Additional substrates will need to be tested to determine whether there is a definitive link between ERAD substrate classification (ERAD-C or ERAD-M) and degree of sensitivity to CTE mutation. Moreover, we define a relatively large minimal cofactor-binding region consisting of TMs 1–9 of Doa10, but we anticipate based on structural modeling that smaller regions of Doa10 directly associate with cofactors. It is likely that the N-terminal TMs are required for proper folding of the cofactor binding site within Doa10. Finally, we analyzed structural predictions of Doa10 using AlphaFold. Although we confirmed the predicted interaction between K119 and E1304 through intragenic suppression, future structural studies will be crucial for further insight into Doa10 and related E3 structures.

STAR★METHODS

Detailed methods are provided in the online version of this paper and include the following:

- KEY RESOURCES TABLE

SUPPLEMENTAL INFORMATION

Supplemental information can be found online at https://doi.org/10.1016/j.isci.2022.105351.

ACKNOWLEDGMENTS

We would like to thank Carolyn Breckel for helpful comments on the manuscript and Shashank Chavali for assistance with AlphaFold. We also thank Phoebe Johnson (deceased) for generating MHY760, Tommer Ravid for generating MHY2935 and MHY2928, and David Adle for generating MHY6527. We also thank Jeffrey Brodsky, Tommer Ravid, and Thomas Sommer for generously providing plasmids and/or antibodies. This work was supported by NIH grant GM136325 to M.H.

AUTHOR CONTRIBUTIONS

A.B.M. and M.H., conceptualization; A.B.M., formal analysis; A.B.M., investigation; A.B.M., writing – original draft; A.B.M. and M.H., writing – review and editing; M.H., supervision; M.H., funding acquisition; M.H., project administration.

DECLARATION OF INTERESTS

The authors declare no competing interests.

INCLUSION AND DIVERSITY

One or more of the authors of this article self-identifies as an underrepresented ethnic minority in their field of research or within their geographical location. Although citing references scientifically relevant for this work, we also actively worked to promote gender balance in our reference list.

Received: May 3, 2022
Revised: August 16, 2022
Accepted: October 11, 2022
Published: November 18, 2022

REFERENCES

Babour, A., Bicknell, A.A., Tourtellotte, J., and Niwa, M. (2010). A surveillance pathway monitors the fitness of the endoplasmic reticulum to control its inheritance. Cell *142*, 256–269. https://doi.org/10.1016/j.cell.2010.06.006.

Bagola, K., von Delbrück, M., Dittmar, G., Scheffner, M., Ziv, I., Glickman, M.H., Ciechanover, A., and Sommer, T. (2013). Ubiquitin binding by a CUE domain regulates ubiquitin chain formation by ERAD E3 ligases. Mol. Cell *50*, 528–539. https://doi.org/10.1016/j.molcel.2013.04.005.

Bazirgan, O.A., and Hampton, R.Y. (2008). Cue1p is an activator of Ubc7p E2 activity in vitro and in vivo. J. Biol. Chem. *283*, 12797–12810. https://doi.org/10.1074/jbc.M801122200.

Biederer, T., Volkwein, C., and Sommer, T. (1997). Role of Cue1p in ubiquitination and degradation at the ER surface. Science *278*, 1806–1809.

Bordallo, J., Plemper, R.K., Finger, A., and Wolf, D.H. (1998). Der3p/Hrd1p is required for endoplasmic reticulum-associated degradation of misfolded lumenal and integral membrane proteins. Mol. Biol. Cell *9*, 209–222.

Braakman, I., and Hebert, D.N. (2013). Protein folding in the endoplasmic reticulum. Cold Spring Harb.Perspect.Biol. *5*, a013201. https://doi.org/10.1101/cshperspect.a013201.

Buchanan, B.W., Lloyd, M.E., Engle, S.M., and Rubenstein, E.M. (2016). Cycloheximide chase analysis of protein degradation in Saccharomyces cerevisiae. J. Vis. Exp. *110*, e53975. https://doi.org/10.3791/53975.

Buchanan, B.W., Mehrtash, A.B., Broshar, C.L., Runnebohm, A.M., Snow, B.J., Scanameo, L.N., Hochstrasser, M., and Rubenstein, E.M. (2019). Endoplasmic reticulum stress differentially inhibits endoplasmic reticulum and inner nuclear membrane protein quality control degradation

pathways. J. Biol. Chem. *294*, 19814–19830. https://doi.org/10.1074/jbc.RA119.010295.

Carvalho, P., Goder, V., and Rapoport, T.A. (2006). Distinct ubiquitin-ligase complexes define convergent pathways for the degradation of ER proteins. Cell *126*, 361–373. https://doi.org/10.1016/j.cell.2006.05.043.

Chen, P., Johnson, P., Sommer, T., Jentsch, S., and Hochstrasser, M. (1993). Multiple ubiquitin-conjugating enzymes participate in the in vivo degradation of the yeast MAT alpha 2 repressor. Cell *74*, 357–369.

Chua, N.K., Howe, V., Jatana, N., Thukral, L., and Brown, A.J. (2017). A conserved degron containing an amphipathic helix regulates the cholesterol-mediated turnover of human squalene monooxygenase, a rate-limiting enzyme in cholesterol synthesis. J. Biol. Chem. *292*, 19959–19973. https://doi.org/10.1074/jbc.M117.794230.

Cohen, I., Wiener, R., Reiss, Y., and Ravid, T. (2015). Distinct activation of an E2 ubiquitin-conjugating enzyme by its cognate E3 ligases. Proc. Natl. Acad. Sci. USA *112*, E625–E632. https://doi.org/10.1073/pnas.1415621112.

Das, R., Mariano, J., Tsai, Y.C., Kalathur, R.C., Kostova, Z., Li, J., Tarasov, S.G., McFeeters, R.L., Altieri, A.S., Ji, X., et al. (2009). Allosteric activation of E2-RING finger-mediated ubiquitylation by a structurally defined specific E2-binding region of gp78. Mol. Cell *34*, 674–685. https://doi.org/10.1016/j.molcel.2009.05.010.

Dederer, V., Khmelinskii, A., Huhn, A.G., Okreglak, V., Knop, M., and Lemberg, M.K. (2019). Cooperation of mitochondrial and ER factors in quality control of tail-anchored proteins. Elife *8*, e45506. https://doi.org/10.7554/eLife.45506.

Deng, M., and Hochstrasser, M. (2006). Spatially regulated ubiquitin ligation by an ER/nuclear membrane ligase. Nature *443*, 827–831. https://doi.org/10.1038/nature05170.

Evans, R., O'Neill, M., Pritzel, A., Antropova, N., Senior, A., Green, T., Žídek, A., Bates, R., Blackwell, S., Yim, J., et al. (2021). Protein complex prediction with AlphaFold-Multimer. Preprint at bioRxiv. https://doi.org/10.1101/2021.10.04.463034.

Finke, K., Plath, K., Panzner, S., Prehn, S., Rapoport, T.A., Hartmann, E., and Sommer, T. (1996). A second trimeric complex containing homologs of the Sec61p complex functions in protein transport across the ER membrane of S. cerevisiae. EMBO J. *15*, 1482–1494.

Flagg, M.P., Wangeline, M.A., Holland, S.R., Duttke, S.H., Benner, C., Neal, S., and Hampton, R.Y. (2021). Inner-nuclear-membrane-associated degradation employs Dfm1-independent retrotranslocation and alleviates misfolded transmembrane-protein toxicity. Mol. Biol. Cell *32*, 521–537. https://doi.org/10.1091/mbc.E20-11-0720.

Foresti, O., Rodriguez-Vaello, V., Funaya, C., and Carvalho, P. (2014). Quality control of inner nuclear membrane proteins by the Asi complex. Science *346*, 751–755. https://doi.org/10.1126/science.1255638.

Foresti, O., Ruggiano, A., Hannibal-Bach, H.K., Ejsing, C.S., and Carvalho, P. (2013). Sterol homeostasis requires regulated degradation of squalene monooxygenase by the ubiquitin ligase Doa10/Teb4. Elife *2*, e00953. https://doi.org/10.7554/eLife.00953.

Furth, N., Gertman, O., Shiber, A., Alfassy, O.S., Cohen, I., Rosenberg, M.M., Doron, N.K., Friedler, A., and Ravid, T. (2011). Exposure of bipartite hydrophobic signal triggers nuclear quality control of Ndc10 at the endoplasmic reticulum/nuclear envelope. Mol. Biol. Cell *22*, 4726–4739. https://doi.org/10.1091/mbc.E11-05-0463.

Gauss, R., Sommer, T., and Jarosch, E. (2006). The Hrd1p ligase complex forms a linchpin between ER-lumenal substrate selection and Cdc48p recruitment. EMBO J. *25*, 1827–1835. https://doi.org/10.1038/sj.emboj.7601088.

Ghaemmaghami, S., Huh, W.K., Bower, K., Howson, R.W., Belle, A., Dephoure, N., O'Shea, E.K., and Weissman, J.S. (2003). Global analysis of protein expression in yeast. Nature *425*, 737–741. https://doi.org/10.1038/nature02046.

Guerriero, C.J., Reutter, K.R., Augustine, A.A., Preston, G.M., Weiberth, K.F., Mackie, T.D., Cleveland-Rubeor, H.C., Bethel, N.P., Callenberg, K.M., Nakatsukasa, K., et al. (2017). Transmembrane helix hydrophobicity is an energetic barrier during the retrotranslocation of integral membrane ERAD substrates. Mol. Biol. Cell *28*, 2076–2090. https://doi.org/10.1091/mbc.E17-03-0184.

Guthrie, C., and Fink, G.R. (2002). Guide to Yeast Genetics and Molecular and Cell Biology (Academic Press), pp. 42–71.

Habeck, G., Ebner, F.A., Shimada-Kreft, H., and Kreft, S.G. (2015). The yeast ERAD-C ubiquitin ligase Doa10 recognizes an intramembrane degron. J. Cell Biol. *209*, 261–273. https://doi.org/10.1083/jcb.201408088.

Hampton, R.Y., Gardner, R.G., and Rine, J. (1996). Role of 26S proteasome and HRD genes in the degradation of 3-hydroxy-3-methylglutaryl-CoA reductase, an integral endoplasmic reticulum membrane protein. Mol. Biol. Cell *7*, 2029–2044.

Huyer, G., Piluek, W.F., Fansler, Z., Kreft, S.G., Hochstrasser, M., Brodsky, J.L., and Michaelis, S. (2004). Distinct machinery is required in Saccharomyces cerevisiae for the endoplasmic reticulum-associated degradation of a multispanning membrane protein and a soluble luminal protein. J. Biol. Chem. *279*, 38369–38378. https://doi.org/10.1074/jbc.M402468200.

Johnson, E.S., Ma, P.C., Ota, I.M., and Varshavsky, A. (1995). A proteolytic pathway that recognizes ubiquitin as a degradation signal. J. Biol. Chem. *270*, 17442–17456. https://doi.org/10.1074/jbc.270.29.17442.

Johnson, P.R., Swanson, R., Rakhilina, L., and Hochstrasser, M. (1998). Degradation signal masking by heterodimerization of MATalpha2 and MATa1 blocks their mutual destruction by the ubiquitin-proteasome pathway. Cell *94*, 217–227.

Jumper, J., Evans, R., Pritzel, A., Green, T., Figurnov, M., Ronneberger, O., Tunyasuvunakool, K., Bates, R., Žídek, A., Potapenko, A., et al. (2021). Highly accurate protein structure prediction with AlphaFold. Nature *596*, 583–589. https://doi.org/10.1038/s41586-021-03819-2.

Kats, I., Khmelinskii, A., Kschonsak, M., Huber, F., Knieß, R.A., Bartosik, A., and Knop, M. (2018). Mapping degradation signals and pathways in a eukaryotic N-terminome. Mol. Cell *70*, 488–501.e5. https://doi.org/10.1016/j.molcel.2018.03.033.

Khmelinskii, A., Blaszczak, E., Pantazopoulou, M., Fischer, B., Omnus, D.J., Le Dez, G., Brossard, A., Gunnarsson, A., Barry, J.D., Meurer, M., et al. (2014). Protein quality control at the inner nuclear membrane. Nature *516*, 410–413. https://doi.org/10.1038/nature14096.

Kim, I., Miller, C.R., Young, D.L., and Fields, S. (2013). High-throughput analysis of in vivo protein stability. Mol. Cell. Proteomics *12*, 3370–3378. https://doi.org/10.1074/mcp.O113.031708.

Kreft, S.G., and Hochstrasser, M. (2011). An unusual transmembrane helix in the endoplasmic reticulum ubiquitin ligase Doa10 modulates degradation of its cognate E2 enzyme. J. Biol. Chem. *286*, 20163–20174. https://doi.org/10.1074/jbc.M110.196360.

Kreft, S.G., Wang, L., and Hochstrasser, M. (2006). Membrane topology of the yeast endoplasmic reticulum-localized ubiquitin ligase Doa10 and comparison with its human ortholog TEB4 (MARCH-VI). J. Biol. Chem. *281*, 4646–4653. https://doi.org/10.1074/jbc.M512215200.

Lips, C., Ritterhoff, T., Weber, A., Janowska, M.K., Mustroph, M., Sommer, T., and Klevit, R.E. (2020). Who with whom: functional coordination of E2 enzymes by RING E3 ligases during poly-ubiquitylation. EMBO J. *39*, e104863. https://doi.org/10.15252/embj.2020104863.

Loayza, D., Tam, A., Schmidt, W.K., and Michaelis, S. (1998). Ste6p mutants defective in exit from the endoplasmic reticulum (ER) reveal aspects of an ER quality control pathway in Saccharomyces cerevisiae. Mol. Biol. Cell *9*, 2767–2784. https://doi.org/10.1091/mbc.9.10.2767.

Matsumoto, S., Nakatsukasa, K., Kakuta, C., Tamura, Y., Esaki, M., and Endo, T. (2019). Msp1 clears mistargeted proteins by facilitating their transfer from mitochondria to the ER. Mol. Cell *76*, 191–205.e10. https://doi.org/10.1016/j.molcel.2019.07.006.

Mehrtash, A.B., and Hochstrasser, M. (2019). Ubiquitin-dependent protein degradation at the endoplasmic reticulum and nuclear envelope. Semin. Cell Dev. Biol. *93*, 111–124. https://doi.org/10.1016/j.semcdb.2018.09.013.

Metzger, M.B., Maurer, M.J., Dancy, B.M., and Michaelis, S. (2008). Degradation of a cytosolic protein requires endoplasmic reticulum-associated degradation machinery. J. Biol. Chem. *283*, 32302–32316. https://doi.org/10.1074/jbc.M806424200.

Metzger, M.B., Pruneda, J.N., Klevit, R.E., and Weissman, A.M. (2014). RING-type E3 ligases: master manipulators of E2 ubiquitin-conjugating enzymes and ubiquitination. Biochim.Biophys. Acta *1843*, 47–60. https://doi.org/10.1016/j.bbamcr.2013.05.026.

Mruk, D.D., and Cheng, C.Y. (2011). Enhanced chemiluminescence (ECL) for routine immunoblotting: an inexpensive alternative to commercially available kits. Spermatogenesis *1*, 121–122. https://doi.org/10.4161/spmg.1.2.16606.

Nakatsukasa, K., Huyer, G., Michaelis, S., and Brodsky, J.L. (2008). Dissecting the ER-associated degradation of a misfolded polytopic membrane protein. Cell *132*, 101–112. https://doi.org/10.1016/j.cell.2007.11.023.

Natarajan, N., Foresti, O., Wendrich, K., Stein, A., and Carvalho, P. (2020). Quality control of protein complex assembly by a transmembrane recognition factor. Mol. Cell *77*, 108–119.e9. https://doi.org/10.1016/j.molcel.2019.10.003.

Neal, S., Jaeger, P.A., Duttke, S.H., Benner, C., Glass, C.K., Ideker, T., and Hampton, R.Y. (2018). The Dfm1 Derlin is required for ERAD retrotranslocation of integral membrane proteins. Mol. Cell *69*, 306–320.e4. https://doi.org/10.1016/j.molcel.2017.12.012.

Nguyen, K.T., Mun, S.H., Yang, J., Lee, J., Seok, O.H., Kim, E., Kim, D., An, S.Y., Seo, D.Y., Suh, J.Y., et al. (2022). The MARCHF6 E3 ubiquitin ligase acts as an NADPH sensor for the regulation of ferroptosis. Nat. Cell Biol. *24*, 1239–1251. https://doi.org/10.1038/s41556-022-00973-1.

Pruneda, J.N., Littlefield, P.J., Soss, S.E., Nordquist, K.A., Chazin, W.J., Brzovic, P.S., and Klevit, R.E. (2012). Structure of an E3:E2∼Ub complex reveals an allosteric mechanism shared among RING/U-box ligases. Mol. Cell *47*, 933–942. https://doi.org/10.1016/j.molcel.2012.07.001.

Rao, B., Li, S., Yao, D., Wang, Q., Xia, Y., Jia, Y., Shen, Y., and Cao, Y. (2021). The cryo-EM structure of an ERAD protein channel formed by tetrameric human Derlin-1. Sci. Adv. *7*, eabe8591. https://doi.org/10.1126/sciadv.abe8591.

Ravid, T., and Hochstrasser, M. (2007). Autoregulation of an E2 enzyme by ubiquitin-chain assembly on its catalytic residue. Nat. Cell Biol. *9*, 422–427. https://doi.org/10.1038/ncb1558.

Ravid, T., Kreft, S.G., and Hochstrasser, M. (2006). Membrane and soluble substrates of the Doa10 ubiquitin ligase are degraded by distinct pathways. EMBO J. *25*, 533–543. https://doi.org/10.1038/sj.emboj.7600946.

Rubenstein, E.M., Kreft, S.G., Greenblatt, W., Swanson, R., and Hochstrasser, M. (2012). Aberrant substrate engagement of the ER translocon triggers degradation by the Hrd1 ubiquitin ligase. J. Cell Biol. *197*, 761–773. https://doi.org/10.1083/jcb.201203061.

Ruggiano, A., Foresti, O., and Carvalho, P. (2014). Quality control: ER-associated degradation: protein quality control and beyond. J. Cell Biol. *204*, 869–879. https://doi.org/10.1083/jcb.201312042.

Ruggiano, A., Mora, G., Buxó, L., and Carvalho, P. (2016). Spatial control of lipid droplet proteins by the ERAD ubiquitin ligase Doa10. EMBO J. *35*, 1644–1655. https://doi.org/10.15252/embj.201593106.

Sato, B.K., Schulz, D., Do, P.H., and Hampton, R.Y. (2009). Misfolded membrane proteins are specifically recognized by the transmembrane domain of the Hrd1p ubiquitin ligase. Mol. Cell *34*, 212–222. https://doi.org/10.1016/j.molcel.2009.03.010.

Satpute-Krishnan, P., Ajinkya, M., Bhat, S., Itakura, E., Hegde, R.S., and Lippincott-Schwartz, J. (2014). ER stress-induced clearance of misfolded GPI-anchored proteins via the secretory pathway. Cell *158*, 522–533. https://doi.org/10.1016/j.cell.2014.06.026.

Scheffer, J., Hasenjäger, S., and Taxis, C. (2019). Degradation of integral membrane proteins modified with the photosensitive degron module requires the cytosolic endoplasmic reticulum-associated degradation pathway. Mol. Biol. Cell *30*, 2558–2570. https://doi.org/10.1091/mbc.E18-12-0754.

Schmidt, C.C., Vasic, V., and Stein, A. (2020). Doa10 is a membrane protein retrotranslocase in ER-associated protein degradation. Elife *9*, e56945. https://doi.org/10.7554/eLife.56945.

Shakya, V.P., Barbeau, W.A., Xiao, T., Knutson, C.S., Schuler, M.H., and Hughes, A.L. (2021). A nuclear-based quality control pathway for non-imported mitochondrial proteins. Elife *10*, e61230. https://doi.org/10.7554/eLife.61230.

Smith, C.E., Tsai, Y.C., Liang, Y.H., Khago, D., Mariano, J., Li, J., Tarasov, S.G., Gergel, E., Tsai, B., Villaneuva, M., et al. (2021). A structurally conserved site in AUP1 binds the E2 enzyme UBE2G2 and is essential for ER-associated degradation. PLoS Biol. *19*, e3001474. https://doi.org/10.1371/journal.pbio.3001474.

Sommer, T., and Jentsch, S. (1993). A protein translocation defect linked to ubiquitin conjugation at the endoplasmic reticulum. Nature *365*, 176–179. https://doi.org/10.1038/365176a0.

Stein, A., Ruggiano, A., Carvalho, P., and Rapoport, T.A. (2014). Key steps in ERAD of luminal ER proteins reconstituted with purified components. Cell *158*, 1375–1388. https://doi.org/10.1016/j.cell.2014.07.050.

Stolz, A., Besser, S., Hottmann, H., and Wolf, D.H. (2013). Previously unknown role for the ubiquitin ligase Ubr1 in endoplasmic reticulum-associated protein degradation. Proc. Natl. Acad. Sci. USA *110*, 15271–15276. https://doi.org/10.1073/pnas.1304928110.

Storici, F., and Resnick, M.A. (2006). The delitto perfetto approach to in vivo site-directed mutagenesis and chromosome rearrangements with synthetic oligonucleotides in yeast. DNA Repair. *409*, 329–345. https://doi.org/10.1016/s0076-6879(05)09019-1.

Swanson, R., Locher, M., and Hochstrasser, M. (2001). A conserved ubiquitin ligase of the nuclear envelope/endoplasmic reticulum that functions in both ER-associated and Matalpha2 repressor degradation. Genes Dev. *15*, 2660–2674.

Szoradi, T., Schaeff, K., Garcia-Rivera, E.M., Itzhak, D.N., Schmidt, R.M., Bircham, P.W., Leiss, K., Diaz-Miyar, J., Chen, V.K., Muzzey, D., et al. (2018). SHRED is a regulatory cascade that reprograms Ubr1 substrate specificity for enhanced protein quality control during stress. Mol. Cell *70*, 1025–1037.e5. https://doi.org/10.1016/j.molcel.2018.04.027.

Tsai, B., Ye, Y., and Rapoport, T.A. (2002). Retro-translocation of proteins from the endoplasmic reticulum into the cytosol. Nat. Rev. Mol. Cell Biol. *3*, 246–255. https://doi.org/10.1038/nrm780.

von Delbruck, M., Kniss, A., Rogov, V.V., Pluska, L., Bagola, K., Löhr, F., Güntert, P., Sommer, T., and Dötsch, V. (2016). The CUE domain of Cue1 aligns growing ubiquitin chains with Ubc7 for rapid elongation. Mol. Cell *62*, 918–928. https://doi.org/10.1016/j.molcel.2016.04.031.

Walter, J., Urban, J., Volkwein, C., and Sommer, T. (2001). Sec61p-independent degradation of the tail-anchored ER membrane protein Ubc6p. EMBO J. *20*, 3124–3131. https://doi.org/10.1093/emboj/20.12.3124.

Weber, A., Cohen, I., Popp, O., Dittmar, G., Reiss, Y., Sommer, T., Ravid, T., and Jarosch, E. (2016). Sequential poly-ubiquitylation by specialized conjugating enzymes expands the versatility of a quality control ubiquitin ligase. Mol. Cell *63*, 827–839. https://doi.org/10.1016/j.molcel.2016.07.020.

Wu, H., Ng, B.S.H., and Thibault, G. (2014). Endoplasmic reticulum stress response in yeast and humans. Biosci.Rep. *34*, e00118. https://doi.org/10.1042/BSR20140058.

Wu, X., Siggel, M., Ovchinnikov, S., Mi, W., Svetlov, V., Nudler, E., Liao, M., Hummer, G., and Rapoport, T.A. (2020). Structural basis of ER-associated protein degradation mediated by the Hrd1 ubiquitin ligase complex. Science *368*, eaaz2449. https://doi.org/10.1126/science.aaz2449.

Zattas, D., Berk, J.M., Kreft, S.G., and Hochstrasser, M. (2016). A conserved C-terminal element in the yeast Doa10 and human MARCH6 ubiquitin ligases required for selective substrate degradation. J. Biol. Chem. *291*, 12105–12118. https://doi.org/10.1074/jbc.M116.726877.

Zelcer, N., Sharpe, L.J., Loregger, A., Kristiana, I., Cook, E.C.L., Phan, L., Stevenson, J., and Brown, A.J. (2014). The E3 ubiquitin ligase MARCH6 degrades squalene monooxygenase and affects 3-hydroxy-3-methyl-glutaryl coenzyme A reductase and the cholesterol synthesis pathway. Mol. Cell Biol. *34*, 1262–1270. https://doi.org/10.1128/MCB.01140-13.

STAR★METHODS

KEY RESOURCES TABLE

REAGENT or RESOURCE	SOURCE	IDENTIFIER
Antibodies		
Mouse monoclonal anti-HA	Sigma-Aldrich	Cat#H9658; RRID: AB_260092
Mouse monoclonal anti-HA	BioLegend	Cat#901513; RRID: AB_2565335
Rabbit polyclonal anti-Ubc6	Walter et al. (2001)	N/A
Mouse monoclonal anti-FLAG	Sigma-Aldrich	Cat#F3165; RRID: AB_259529
Mouse monoclonal anti-Myc	Covance	Cat#MMS-150R; RRID: AB_291325
Rabbit anti-Doa10 serum	Kreft et al. (2006)	N/A
Mouse monoclonal anti-PGK	ThermoFisher	Cat#459250; RRID: AB_2532235
Rabbit monoclonal anti-G6PDH	Sigma-Aldrich	Cat#A9521; RRID: AB_258454
Rabbit anti-Cue1 serum	Cohen et al. (2015)	N/A
Bacterial and virus strains		
Escherichia coli TOP10F' Competent Cells	ThermoFisher	Cat#C303003
Chemicals, peptides, and recombinant proteins		
Cycloheximide	Sigma-Aldrich	Cat#01810
PMSF	AmericanBio	Cat#329-98-6
Aprotonin	Roche	Cat#10236624001
cOmplete protease inhibitor tablet	Roche	Cat#11697498001
Digitonin	EMD Millipore	Cat#300410
Immobilized Protein A	RepliGen	Cat#IPA300
Experimental models: Organisms/strains		
Saccharomyces cerevisiae MHY500 (DF5)	Chen et al. (1993)	N/A
Saccharomyces cerevisiae JY103 (YPH499-derived)	Swanson et al. (2001)	N/A
Additional yeast strains used: refer to Table S1		
Recombinant DNA		
Plasmids used: refer to Table S2.		
Software and algorithms		
AlphaFold2	Jumper et al. (2021)	https://alphafold.ebi.ac.uk
AlphaFold-Multimer	Evans et al. (2021)	N/A
Prism 9 for Mac	GraphPad Software	https://www.graphpad.com/scientific-software/prism/

RESOURCE AVAILABILITY

Lead contact

Requests for materials and resources can be directed to the lead contact, Mark Hochstrasser, Yale University (mark.hochstrasser@yale.edu).

Materials availability

All unique/stable reagents generated in this study are available from the leader contact on request.

Data and code availability

- All data reported in this article will be shared by the lead contact on request.
- This article does not report original code.

- Additional information required to reanalyze the data reported in this article is available by the lead contact on request.

EXPERIMENTAL MODEL AND SUBJECT DETAILS

All strains in this study are derived from either the MHY500 (Chen et al., 1993) or JY103 (YPH499-derived) background (Swanson et al., 2001).

METHOD DETAILS

Yeast methods

Yeast were genetically manipulated using standard techniques and grown at 30°C for all experiments. Yeast rich (YPD) and minimal (SD) media were prepared as described (Guthrie and Fink, 2002). For the degradation-sensitive growth assays, cells were grown in selective medium overnight. Each culture was diluted to an OD_{600} of 0.2, and 5-fold serial dilutions were made. Diluted cultures were spotted onto minimal media plates and incubated for 2–3 days.

Yeast strain and plasmid methods

Strains and plasmids used in this study are listed in Tables S1 and S2, respectively. C-terminal truncation mutants of Doa10 were constructed using a similar approach described previously (Zattas et al., 2016). The deletion cassettes for the N-terminal truncation mutants of Doa10 were generated by two sequential PCRs. In the first reaction, genomic DNA from MHY10842 was used as template for generating the various N-terminal truncation variants of *doa10(1–1000)*; these PCR products also contained an ATG start codon, a selectable marker, and homology (~250bp) to the *DOA10* terminator. Homology to the *DOA10* promoter (~70bp) was added in the forward primer for the second reaction. The deletion cassettes were then transformed into a *doa10Δ* haploid strain (MHY10818) and integrated at the *doa10Δ* locus. Transformants were crossed with MHY3054, and strains were confirmed by PCR and proper expression by immunoblotting. The deletion cassette for MHY11333 (*doa10(1-1080-CTE)*) was also generated by two PCR reactions. First, the CTE-13myc cassette was amplified from MHY8655. Second, homology was added to this cassette to enable integration following codon 1080 of *DOA10* in the yeast genome. Finally, the cassette was transformed into JY112 and the resulting transformant was crossed with JY103. The yeast strains containing CTE or TM1 mutations were made using SceI-mediated *delitto perfetto* (Storici and Resnick, 2006). This was performed in MHY12186, MHY12449, or MHY12494 with DNA generated from digestion of the p414-GPD-doa10_1198-1319 or pRS316-doa10_1-310 variants. All mutants were verified by PCR and proper expression by immunoblotting (S10-S13).

Standard techniques were used for recombinant DNA work in *Escherichia coli* (Rubenstein et al., 2012). We generated YCplac33-Ub_{G76V}-Ubc6-HA (C87A) by subcloning a BspEI/HindIII fragment from pRS416-Ubc6-HA-C87A into pTR1650 (Sommer and Jentsch, 1993; Weber et al., 2016). All other plasmids in this study were generated by restriction digest and ligation of MHY500-derived PCR products or QuikChange mutagenesis.

Antibodies and immunoblotting

Immunoblotting was performed as described (Buchanan et al., 2019). The following antibodies were used for immunoblotting: mouse anti-HA (H9658, Sigma) at 1:2,000; rabbit anti-Ubc6 (gift from Thomas Sommer) (Walter et al., 2001) at 1:10,000; mouse anti-FLAG (F3165; Sigma) at 1:10,000; mouse anti-HA (16B12, BioLegend) at 1:1,000; mouse anti-MYC (9E10, Covance) at 1:10,000; rabbit anti-Doa10 at 1:2,000 (Kreft et al., 2006); rabbit anti-Cue1 at 1:2,000 (Cohen et al., 2015); mouse anti-PGK (459250, Thermo Fisher) at 1:20,000; rabbit anti-G6PDH (A9521, Sigma) at 1:20,000. Primary antibody incubations were followed with either peroxidase-coupled sheep anti-mouse or peroxidase-coupled goat anti-rabbit secondary antibodies (GE Healthcare) at 1:10,000 and visualized by enhanced chemiluminescence (Mruk and Cheng, 2011) with imaging on a G:Box system (Syngene).

Cycloheximide-chase assays and protein extraction

Cycloheximide (CHX)-chase assays were performed as described previously (Buchanan et al., 2016; Huyer et al., 2004). Briefly, yeast cells were grown in YPD or selective SD media at 30°C to mid-exponential phase. 12.5 OD_{600} units were harvested and CHX was added to a final concentration of 0.25 mg/mL. For each timepoint, ~2.5 OD_{600} units were taken, diluted in cold stop mix (20 mM sodium azide) to a final concentration

of 10 mM sodium azide, and kept on ice until the end of the chase. Cells were then lysed using the alkaline lysis method (Buchanan et al., 2016) and in some cases, trichloroacetic acid (TCA) precipitation was performed following cell lysis (Huyer et al., 2004). Whole cell lysates or TCA pellets were resuspended in 2X Laemmli sample buffer or TCA sample buffer, respectively, and incubated at 37°C for 30 min. Protein samples were centrifuged to remove precipitated material and then separated by SDS-PAGE and analyzed by western blot.

Co-immunoprecipitation analysis

Yeast co-immunoprecipitation (co-IP) analyses were performed using a previously described method with minor modifications (Kreft and Hochstrasser, 2011). Yeast cells were grown in YPD or selective SD media to mid-exponential phase and 35 OD_{600} units were harvested by centrifugation. All of the following steps were performed at 4°C or on ice. Cell pellets were resuspended in 0.6 mL cold extraction buffer (50 mM Tris pH 7.5) with protease inhibitors PMSF (1 mM) and aprotonin (5 μg/mL) and disrupted using glass bead lysis. Lysates were diluted with 0.4 mL extraction buffer and cleared by centrifugation for 5 min at 400 ×*g*. The crude microsomal fraction was isolated by centrifugation for 10 min at 16,000 ×*g* and resuspended in 0.5 mL resuspension buffer (RB) (50 mM Tris pH 7.5, 200mM NaCl, 10% glycerol, with protease inhibitors (PMSF (1 mM), aprotonin (5 μg/mL), and cOmplete protease inhibitor tablet). Membranes were solubilized in 1% digitonin for 10 min on ice and then subject to centrifugation for 10 min at 16,000 ×*g*. Following centrifugation, the supernatant was diluted 1:1 in RB and an aliquot (1.5% total) was taken for the input. Rabbit anti-Doa10 serum was added to the diluted supernatant and incubated for 2 h with gentle agitation. Afterwards, protein A-Sepharose beads were added and incubated for an additional hour. Beads were washed four times with RB without protease inhibitors. Proteins were eluted following addition of 40μL 2X Laemmli sample buffer and incubation at 37°C for 30 min. Eluted samples were analyzed by SDS-PAGE and immunoblotting.

AlphaFold structure prediction

The predicted structure of *S. cerevisiae* Doa10 was obtained from the AlphaFold protein structure database (https://alphafold.ebi.ac.uk). The predicted structure of the Doa10-N1314A mutant protein was processed using the high-performance computing (HPC) cluster at Yale with the open source code for AlphaFold2 (Jumper et al., 2021). The maximum template release date used was 2020-05-14. The predicted structure of the *S. cerevisiae* Doa10 complex, which included full-length Doa10, Ubc6, Cue1, and Ubc7, was processed by the Yale HPC with the open source code for AlphaFold-Multimer (Evans et al., 2021). The maximum template release date used was 2021-12-01 with the settings "–model_preset=multimer", "–db_preset=full_dbs", and "–is_prokaryote_list=false".

QUANTIFICATION AND STATISTICAL ANALYSIS

All data is represented as ± SEM from three or four experiments. Band intensities from immunoblotting were quantified using Gene Tools (Syngene) and normalized to the loading control. Statistical analysis was performed using GraphPad Prism. For CHX-chase experiments involving two strains, two-way ANOVA with Bonferroni's post hoc analysis was applied to compare data. For experiments involving at least three strains, two-way ANOVA with Tukey's post hoc analysis was applied for data comparison. Significance was indicated as following: ns, not significant; *$p < 0.05$; **$p < 0.01$; ***$p < 0.001$; ****$p < 0.0001$.